

1 **Cohesin facilitates zygotic genome activation in zebrafish**

2 Michael Meier<sup>1</sup>, Jenny Grant<sup>1</sup>, Amy Dowdle<sup>1</sup>, Amarni Thomas<sup>1</sup>, Jennifer Gerton<sup>2,3</sup>, Philippe

3 Collas<sup>4</sup>, Justin M. O'Sullivan<sup>5,6</sup>, Julia A. Horsfield<sup>1,6\*</sup>

4

5 <sup>1</sup>Department of Pathology, University of Otago, Dunedin 9016, New Zealand.

6 <sup>2</sup>Stowers Institute for Medical Research, 1000 E 50<sup>th</sup> Street, Kansas City, Missouri 64110,

7 USA.

8 <sup>3</sup>Department of Biochemistry and Molecular Biology, University of Kansas Medical Center,

9 Kansas City, KS 66160, USA.

10 <sup>4</sup>Department of Molecular Medicine, Institute of Basic Medical Sciences, Faculty of Medicine,

11 University of Oslo, Norway.

12 <sup>5</sup>Liggins Institute, The University of Auckland, Private Bag 92019, Auckland, New Zealand.

13 <sup>6</sup>Maurice Wilkins Centre for Molecular Biodiscovery, The University of Auckland, Private Bag

14 92019, Auckland, New Zealand.

15

16

17 \*To whom correspondence should be addressed at the University of Otago, Dunedin School

18 of Medicine, Department of Pathology, 58 Hanover Street, Dunedin 9016, New Zealand.

19 Tel +64 3 479 7436. Email: [julia.horsfield@otago.ac.nz](mailto:julia.horsfield@otago.ac.nz).

20

21

22 **Abstract**

23

24 At zygotic genome activation (ZGA), changes in chromatin structure are associated with new  
25 transcription immediately following the maternal-to-zygotic transition (MZT). The nuclear  
26 architectural proteins, cohesin and CCCTC-binding factor (CTCF), contribute to chromatin  
27 structure and gene regulation. We show here that normal cohesin function is important for  
28 ZGA in zebrafish. Depletion of cohesin subunit Rad21 delays ZGA without affecting cell  
29 cycle progression. In contrast, CTCF depletion has little effect on ZGA whereas complete  
30 abrogation is lethal. Genome wide analysis of Rad21 binding reveals a change in distribution  
31 from pericentromeric satellite DNA, and few locations including the *miR-430* locus (whose  
32 products are responsible for maternal transcript degradation), to genes, as embryos  
33 progress through the MZT. After MZT, a subset of Rad21 binding occurs at genes  
34 dysregulated upon Rad21 depletion and overlaps pioneer factor Pou5f3, which activates  
35 early expressed genes. Rad21 depletion disrupts the formation of nucleoli and RNA  
36 polymerase II foci, suggestive of global defects in chromosome architecture. We propose  
37 that Rad21/cohesin redistribution to active areas of the genome is key to the establishment  
38 of chromosome organization and the embryonic developmental program.

39

40

41

## 42 **Author Summary**

43 During the first few hours of existence, early zygotic cellular events are regulated by  
44 maternally inherited molecules. From a defined timepoint, the zygotic genome gradually  
45 becomes active and is transcribed. How the zygotic genome is first held inactive before  
46 becoming rapidly activated is poorly understood. Both gene repression and activation  
47 mechanisms are involved, but one aspect that has not yet been investigated is how 3-  
48 dimensional chromosome structure influences genome activation. In this study, we used  
49 zebrafish embryos to model zygotic genome activation.

50

51 The multi-subunit protein complex, cohesin, and the DNA-binding protein CCCTC-binding  
52 factor (CTCF) both have well known and overlapping roles in 3-dimensional genome  
53 organization. We depleted cohesin subunit Rad21, or CTCF, to determine their effects on  
54 zygotic genome activation. Moderate Rad21 depletion delayed transition to zygotic gene  
55 expression, without disrupting the cell cycle. By contrast, moderate CTCF depletion had very  
56 little effect; however, strong depletion of CTCF was lethal. We surveyed genome-wide  
57 binding of Rad21 before and after the zygotic genome is activated, and determined what  
58 other chromatin factors and transcription factors coincide with Rad21 binding. Before  
59 genome activation, Rad21 was located at satellite DNA and a few noncoding genes, one of  
60 which (*miR-430*) is responsible for degrading maternal transcripts. Following genome  
61 activation, there was a mass relocation of Rad21 to genes, particularly active genes and  
62 those that are targets of transcriptional activators when the zygotic genome is switched on.  
63 Depletion of Rad21 also affected global chromosome structure.

64

65 Our study shows that cohesin binding redistributes to active RNA Polymerase II genes at the  
66 onset of zygotic gene transcription. Furthermore, we suggest that cohesin contributes to  
67 dynamic changes in chromosome architecture that occur upon zygotic genome activation.

68

## 69 **Introduction**

70

71 Zygotic genome activation (ZGA) establishes, for the first time in a zygote, a genome that is  
72 competent for transcription (Blythe and Wieschaus, 2015; Fassnacht and Ciosk, 2017;  
73 Onichtchouk and Driever, 2016; Palfy et al., 2017; Svoboda et al., 2015). ZGA involves the  
74 transfer of maternal to zygotic control of embryonic development.

75

76 Commensurate with ZGA, maternal transcripts must be degraded at the maternal to zygotic  
77 transition (MZT) (Marco, 2017). In zebrafish, many maternal transcripts are targeted for  
78 degradation by *miR-430*, which is among the few early expressed transcripts in the embryo  
79 (Bazzini et al., 2012; Giraldez et al., 2006). Other maternal RNAs are N6-methyladenosine  
80 (m6A) modified, and are cleared by an m6A-binding protein, Ythdf2 (Zhao et al., 2017).

81 Unique RNA-binding proteins also play a role in controlling RNA metabolism and turnover  
82 during MZT (Despic et al., 2017). Therefore, clearance of maternal RNA is essential for  
83 transition to the zygotic transcription program.

84

85 Mechanisms regulating both transcriptional activation and transcriptional repression are  
86 thought to control ZGA in the early embryo (Joseph et al., 2017; Lee et al., 2013;  
87 Onichtchouk and Driever, 2016). Evidence from *Xenopus* and zebrafish suggests the  
88 existence of a titratable, maternally deposited repressor that initially holds the transcription of  
89 the zygotic genome in check (Kimelman et al., 1987; Newport and Kirschner, 1982b; Nothias  
90 et al., 1995). In *Xenopus*, ZGA coincides with a dramatic increase in the nucleus-to-  
91 cytoplasm (N:C) volume ratio (Jevtic and Levy, 2015; Newport and Kirschner, 1982a).

92 Increasing the N:C ratio by the addition of extra DNA (Newport and Kirschner, 1982b) or by  
93 injection of scaffolding proteins (Jevtic and Levy, 2015) accelerates ZGA. An *in vitro* study in  
94 *Xenopus* egg extracts showed that histones H3 and H4 are strong candidates for the  
95 maternal repressor activity (Amodeo et al., 2015); transcription repression by H3/H4 could

96 be manipulated *in vitro* by altering the ratio of DNA template to histone quantities alone. In  
97 zebrafish, core histones outcompete transcription factors for access to the genome, thereby  
98 regulating the onset of transcription (Joseph et al., 2017). These studies suggest that  
99 transcription is activated as the histone repressors are titrated out during successive cell  
100 divisions. Therefore, up until ZGA, repression mechanisms counteract factors that activate  
101 transcription in the embryo.

102

103 Transcriptional activation at ZGA appears to involve a combination of ‘pioneer’ transcription  
104 factor activity, and a gain in active chromatin modifications. At the zebrafish maternal-to-  
105 zygotic transition (MZT), distinctive histone modifications appear (Andersen et al., 2013;  
106 Vastenhouw and Schier, 2012; Vastenhouw et al., 2010), and nucleosomes become strongly  
107 positioned at promoters (Zhang et al., 2014b). Even before ZGA, the zebrafish genome is  
108 marked with modified histones (Lindeman et al., 2011) and specific sites of DNA methylation  
109 (Jiang et al., 2013; Potok et al., 2013). However, although chromatin modifications can  
110 demarcate active regions of transcription, additional factors are usually needed for  
111 transcription activation (Hontelez et al., 2015). Sequence-specific transcription factors  
112 operating at ZGA vary between species. In *Drosophila*, the zinc finger protein, Zelda,  
113 activates many early genes (Harrison et al., 2011; Li et al., 2014). In zebrafish, Nanog,  
114 Pou5f3 (also called Oct4) and SoxB1 regulate expression of early zygotic genes (Lee et al.,  
115 2013; Leichsenring et al., 2013; Onichtchouk and Driever, 2016). Recently, the DUX family  
116 of transcription factors was found to activate zygotic genes in mice (De Iaco et al., 2017;  
117 Hendrickson et al., 2017; Whiddon et al., 2017).

118

119 Global chromatin structure is also linked to transcription activation; for example, formation of  
120 architectural features such as topologically associated domains (TADs) mark the onset of  
121 transcription in the mouse embryo (Flyamer et al., 2017; Lu et al., 2016). In *Drosophila*,  
122 chromatin architecture in the form of TADs emerges at ZGA independently of gene

123 transcription (Hug et al., 2017). This is consistent with the idea that genome structure  
124 formation precedes transcription (Krijger and de Laat, 2017). Chromatin structure in turn  
125 influences the binding of transcription factors and RNA Polymerase II (RNAPII) (Newman  
126 and Young, 2010).

127

128 While individual players in ZGA may vary between species, a universal theme is that the  
129 spatial organization of chromosomes changes as cells commit to developmental fates (de  
130 Wit et al., 2013; Hug et al., 2017; Phillips-Cremins, 2014; Vietri Rudan et al., 2015). Spatial  
131 organization of the genome depends in part on the nuclear architectural proteins, cohesin  
132 and CCCTC-binding factor (CTCF), which contribute to the 3-dimensional (3D) organization  
133 of chromosomes (Vietri Rudan and Hadjur, 2015), and the formation of DNA loops within  
134 TADs (Giorgetti et al., 2014; Hug et al., 2017; Van Bortle et al., 2014; Vietri Rudan et al.,  
135 2015). Compartmentalization of active and inactive regions of the genome does not depend  
136 on CTCF (Nora et al., 2017) or cohesin (Merkenschlager and Nora, 2016). However, local  
137 spatial organization within TADs can facilitate transcription of developmental loci (Ferraiuolo  
138 et al., 2010; Narendra et al., 2015; Rousseau et al., 2014), thereby determining cell fate and  
139 driving embryo development.

140

141 In this study, we asked whether cohesin and CTCF contribute to ZGA. We found that  
142 cohesin (but not CTCF) depletion delays ZGA, and that chromosome bound cohesin  
143 spreads from satellite and non-coding DNA to genes when the zygotic genome becomes  
144 activated. A fraction of gene-associated cohesin binding sites are co-occupied by 'pioneer'  
145 transcription factors Pou5f3 and Sox2, and enriched for active histone marks. We propose  
146 that cohesin plays a crucial role in organizing a chromatin structure that is permissive for  
147 transcription at ZGA.

148

149

150

## 151 **Results**

152

### 153 **Depletion of cohesin and CTCF in zebrafish embryos**

154 As embryos progress through MZT at 3.3 hours post-fertilization (hpf), the main wave of  
155 zygotic gene transcription is activated (Fig. 1A, Heyn et al. (2014)). Relatively low levels of  
156 Rad21 (~100) and CTCF (~150) transcripts are present pre-ZGA, with both transcript and  
157 protein levels increasing by 2-3-fold in the main wave of ZGA (Fig. 1B,C). Genes encoding  
158 Rad21 and CTCF are essential for cell survival (Nasmyth and Haering, 2005) (including  
159 germ cells), which limits the genetic tools available for their manipulation. We previously  
160 bypassed homozygous lethality by using morpholino oligonucleotides (MO) to tightly titrate  
161 the levels of Rad21 and CTCF (Marsman et al., 2014; Rhodes et al., 2010; Schuster et al.,  
162 2015). Here, we were able to substantially reduce the protein levels of cohesin subunit  
163 Rad21 and CTCF in early embryos in order to assess their effects on zygotic genome  
164 activation (Figs 1, S1, S1E). Rad21-depleted embryos were rescued by a transcript  
165 encoding wild type Rad21, but not by mutant Rad21 containing the *rad21<sup>nz171</sup>* nonsense  
166 mutation (Horsfield et al., 2007) (Fig. S2).

167

168 MOs injected at the 1-cell stage reduced protein levels of Rad21 and CTCF by 40-80%,  
169 even pre-ZGA (Figs 1D, S1). By the 4.5 hpf 'dome' stage, Rad21-depleted embryos had just  
170 slightly fewer cells than wild type, although the difference was not significant ( $p = 0.1138$ ,  
171 unpaired *t*-test) (Fig. S3A). Analysis of cell cycle status by flow cytometry showed that both  
172 wild-type and Rad21-depleted embryos had a large majority of cells with 2N DNA content,  
173 although the Rad21-depleted embryos had an increase in cells with 4N DNA content, from  
174 7% in wildtype to 10% with Rad21 depletion (Fig. S3B). Surviving CTCF-depleted embryos  
175 displayed similar cell cycle profiles to wild type (data not shown). However, many CTCF MO-

176 injected embryos died pre-MZT, suggesting that survivors had sub-threshold CTCF  
177 depletion.

178

### 179 **Rad21 depletion delays the onset of the zygotic transcription program**

180 To determine the effects Rad21 and CTCF depletion on zygotic transcription, we used RNA-  
181 seq to analyse the transcriptome of untreated embryos (referred to here as ‘wild type’) and  
182 embryos treated with Rad21- or CTCF-targeting MOs. Five developmental stages were  
183 analyzed spanning pre-MZT (2.5 hpf), MZT (3.3 hpf), and post-MZT (4.5 and 5.3 hpf) stages  
184 up to the tailbud stage (10 hpf). The sample-to-sample distances between the expression  
185 profiles were calculated (R package DESeq2) to cluster time points and treatments. A  
186 graphical representation of the sample-to-sample distance is shown in a principal component  
187 (PCA) plot in Figure 2A. We found that Rad21 depletion results in a complement of  
188 transcripts that appear delayed in developmental timing relative to wild type at the post-MZT  
189 stages of 4.5 and 5.3 hpf (PC1, Fig. 2A). By contrast, profiles from CTCF-depleted embryos  
190 cluster similarly to wild type embryos from the same stage (Fig. 2A).

191

### 192 **More transcripts are affected following depletion of Rad21 than of CTCF**

193 We identified differentially represented transcripts between wild type, Rad21- and CTCF-  
194 depleted embryos at each of the five stages (Table S1). Rad21 and CTCF depletion most  
195 robustly affected transcript levels post ZGA at 4.5 hpf and 5.3 hpf (Fig. 2B). We next  
196 annotated (Lee et al., 2013) the origin of the differentially represented transcripts (maternal,  
197 weakly maternal or zygotic) in Rad21-depleted embryos and CTCF-depleted embryos  
198 compared to wild type at the 4.5 hpf ‘dome stage’. We found that upon Rad21 depletion,  
199 3,285 differentially represented transcripts (FDR=0.05) were both maternal and zygotic, with  
200 maternal transcripts more abundant relative to wild type and zygotic transcripts under-  
201 represented (Fig. 2C, Table S1), suggesting ZGA is delayed. Following CTCF depletion,



202 there were 888 differentially represented transcripts, almost 4-fold fewer than observed upon  
203 Rad21 depletion (FDR=0.05) (Fig. 2D, Table S1).

204

205 We then plotted the expression levels of differentially expressed transcripts identified from  
206 dome stage at all time points sampled. Transcripts that are under-represented in Rad21-  
207 depleted embryos normally increase over developmental time in wild type, and transcripts  
208 that are over-represented upon Rad21 depletion are reduced over time in wild type embryos  
209 (Fig. 3A,B), with significantly more transcripts affected when compared to CTCF depletion  
210 (Fig. S4). CTCF-depleted embryos showed a similar trajectory of differentially represented  
211 transcripts over developmental time (Fig. S4A,B). Following Rad21 depletion, delay in the  
212 expression of individual zygotic genes was confirmed by quantitative PCR (Fig. 3C).

213 Furthermore, expression of these genes was similarly delayed by depletion of a second  
214 cohesin subunit, Smc3 (Fig. 3C, Fig. S1E), suggesting that the effect of Rad21 depletion on  
215 ZGA is mediated through abolition of cohesin complex function. We conclude that even  
216 partial depletion of cohesin causes a delay in zygotic genome activation.

217

218 While transcripts that are differentially represented upon Rad21 depletion were assignable to  
219 functional pathways (Fig. 4), transcripts responding to CTCF depletion were not. At the 4.5  
220 hpf 'dome' stage, transcripts under-represented upon Rad21 depletion are involved in  
221 ribosome assembly, translation and RNA metabolism functions (Fig. 4A, Table S2). Over-  
222 represented transcripts reflect the maternal RNA landscape and are involved in energy  
223 systems and mitochondrial functions (Fig. 4B, Table S2).

224

225 The RNA-seq data indicate that Rad21 (but not CTCF) depletion led to a delay in  
226 degradation of maternal mRNAs in combination with a delay in activation of zygotic genes,  
227 when compared to stage-matched embryos of equivalent morphology and cell number to

228 wild type. Overall, our data suggests that cohesin is necessary for the timely transition to,  
229 and promotion of, maternal to zygotic transcription programs.

230

### 231 **Rad21 binding redistributes through ZGA**

232 Considering the importance of Rad21/cohesin for progression to the zygotic transcription  
233 program (Figs 2-4), we decided to further investigate Rad21 function during ZGA. To  
234 determine the distribution of Rad21 on chromosomes in early development, we conducted  
235 chromatin immunoprecipitation followed by high throughput sequencing (ChIP-seq) in wild  
236 type embryos at 2.5, 4.5 and 10 hpf with custom antibodies against zebrafish Rad21  
237 (Rhodes et al., 2010) (Fig. S5). At 2.5 hpf pre-ZGA, 2,011 enriched Rad21 peaks were  
238 detected on chromosomes. After ZGA, there was significant recruitment of Rad21 to  
239 chromosomes that increased over developmental time (Fig. 5A). By the 4.5 hpf 'dome'  
240 stage, wild type embryos had accumulated 7,144 significant Rad21 binding peaks, and by 10  
241 hpf, there were 18,075 peaks in total. During ZGA and early development, Rad21 peak  
242 distribution shifts closer to the transcription start sites (TSS) of genes (Fig. 5A). The data  
243 suggest that pre-ZGA, Rad21/cohesin binds to few loci and is mostly excluded from genes,  
244 whereas post-ZGA, Rad21 binding accumulates at gene-dense regions. We performed  
245 ATAC-seq (Buenrostro et al., 2015) on wild type embryos at 2.5 hpf to determine if Rad21  
246 binds to open chromatin regions at pre-ZGA. About half the accessible chromatin sites at 2.5  
247 hpf also recruit Rad21 (Fisher's exact test, right tail:  $p \leq 1.00^{-20}$ ) (Fig. 5B), indicating that a  
248 subset of cohesin binding sites are located in the very few regions, 337 in total, which are  
249 accessible pre-ZGA. About 90% of the overlapping accessible regions correspond with  
250 satellite DNAs (Table S3; specific examples are shown in Fig. S6).

251

252 The remarkable redistribution of Rad21 binding to genes post-ZGA is exemplified by its  
253 recruitment at chromosome 4 (Fig. 5C). The long arm of chromosome 4 is gene-poor, has  
254 extensive heterochromatin, and replicates late. High densities of 5S ribosomal DNA (rDNA),

255 small nuclear RNAs (snRNAs), half of all tRNAs, and 30% of all zinc finger domain genes  
256 are present on the long arm of chromosome 4 (Howe et al. 2013). Prior to ZGA, many of  
257 these loci were enriched for Rad21 (right side), whereas the RNAPII gene-rich region of  
258 chromosome 4 (left side) excluded Rad21 binding (Fig. 5C). Post-ZGA, Rad21 binding  
259 became increasingly enriched at the RNAPII gene-rich region of chromosome 4, and some  
260 of its pre-ZGA binding sites were lost (Fig. 5C).

261

262 Genes that recruit Rad21 pre-ZGA (within a 20 kb window) included *hsp70l*, *sox2*, *gata2a*  
263 and the *miR-430* complex (Fig. S7); and multiple zinc finger domain encoding proteins  
264 located on chromosome 4 (Fig. S8). Transcripts from *miR-430* and zinc finger domain  
265 encoding genes are expressed as early as the 64-cell stage, prior to the main wave of  
266 zygotic transcription (Heyn et al. 2014). The mature *miR-430* microRNAs mark a substantial  
267 amount of maternally deposited transcripts for degradation (Giraldez 2006). Interestingly,  
268 many zinc finger encoding genes marked by Rad21 binding are not expressed until post-  
269 ZGA (Fig. S8).

270

271 Besides association with regions on the long arm of chromosome 4, 41% (824/2,011) of the  
272 Rad21 peaks were found at satellite elements (satDNAs) located at pericentromeric regions  
273 of the genome (Figs 5D,E; S6, Table 1). Further classification of these elements shows that  
274 BRSATI and SAT-1 were among the highest enriched members of satDNAs found at Rad21  
275 sites pre-ZGA representing over 70% of satDNAs identified. satDNAs represent less than  
276 1% of the genome in zebrafish and are therefore significantly enriched ( $p$  value  $< 1.0^{-20}$ ,  
277 Fisher's exact test) in the 2.5 hpf Rad21 peaks, whereas DNA transposons are relatively  
278 abundant accounting for 33% of the genome and are not significantly enriched. Long  
279 terminal repeats (LTRs) and rRNAs are also significantly enriched in pre ZGA Rad21 peaks  
280 (Table 1).

281

## 282 **Rad21 locates to genes upon genome activation**

283 After ZGA, there was significant recruitment of Rad21 to chromosomes that increased over  
284 developmental time (Fig. 5A). By the 4.5 hpf 'dome' stage, wild type embryos had  
285 accumulated 7,144 significant Rad21 binding peaks including ~3,000 that were gene-  
286 associated, and by 10 hpf, there were 18,075 peaks in total with 5,937 gene-associated  
287 (Figs 5A, 6A, Table S3). Rad21 binding was significantly over-represented in coding regions  
288 after ZGA. Furthermore, Rad21 binding was particularly enriched at promoters and 5'  
289 untranslated regions (5' UTR), as well as to exons, transcription termination sites (TTS), and  
290 3' UTRs (Fig. 6A).

291

292 Overall, 12% (293/2371) of over-represented transcripts, and 15% (179/1185) of under-  
293 represented transcripts were derived from genes that recruited Rad21 (Fig. 6B), implying the  
294 corresponding genes could be directly regulated by Rad21. The association of differential  
295 expression with bound genes is significant (Fig. 6B), even though relatively few dysregulated  
296 genes are bound. We used *k*-means clustering ( $k=2$ ) to visualize Rad21 binding profiles over  
297 two subsequent developmental stages (4.5 and 10 hpf). About half of the regulated genes  
298 that contained Rad21 binding (58% for under-represented transcripts and 52% for over-  
299 represented) had lost that binding by 10 hpf (Fig. 6C,D), indicating that Rad21 is likely to be  
300 specifically associated with those genes during ZGA, and potentially involved in their direct  
301 regulation at that time. Following Rad21 depletion, when compared with over-represented  
302 transcripts, genes with under-represented transcripts at 4.5 hpf had higher transcription  
303 levels in wild type embryos by 10 hpf, irrespective of Rad21 binding (Fig. 6E). Only a small  
304 fraction (5-8%) of genes with over-represented transcripts at 4.5 hpf also showed altered  
305 expression at 10 hpf. Genes found to be downregulated at 4.5 hpf were more likely to also  
306 be differentially expressed at 10 hpf (14%), but there was no difference between genes that  
307 gain or lose Rad21 binding at 10 hpf (Fig. 6F, clusters I and II, respectively). This indicates  
308 that a small subset of genes bound by Rad21 during ZGA are affected later in development

309 by Rad21 depletion. However, although it is likely that some of the bound genes may be  
310 regulated directly, a larger fraction appears to be regulated indirectly.

311

312 Our results indicate that Rad21 is present at repetitive sequences and ncRNA genes prior to  
313 ZGA, with a transition to RNAPII genes at ZGA, once transcription starts. The marked  
314 enrichment of Rad21 at genes through developmental time suggests that cohesin may  
315 facilitate their expression. However, because many more genes are regulated by Rad21  
316 depletion than are bound by Rad21, it is unlikely that direct gene regulation by cohesin  
317 explains the delay in ZGA.

318

319 **Rad21 binding coincides with active histone marks and sites occupied by**  
320 **pluripotency factors Pou5f3 and Sox2**

321 To further investigate a possible role for Rad21 in ZGA, we sought to determine if Rad21  
322 binding coincides with other hallmarks of gene activation, including H3K4me1 and H3K27ac  
323 enhancer modifications, H3K4me3 marks associated with active gene promoters, and  
324 H3K27me3 modification of polycomb-repressed genes (Vastenhouw and Schier, 2012). For  
325 this analysis, we surveyed defined regions centered on Rad21 binding sites for enrichment  
326 of these modified histones by comparing Rad21 ChIP-seq data to publically available histone  
327 ChIP-seq data (Bogdanovic et al., 2012; Zhang et al., 2014b) at peri-ZGA time points. (Fig.  
328 7A). 48% of the Rad21 peaks (3,416/7,144) overlapped with at least one of the enhancer  
329 and promoter associated marks, H3K4me1, H3K4me3 and H3K27ac (hypergeometric test,  $p$   
330  $\leq 2.72^{-2803}$ ) (Fig. 7A, Table S4). A smaller set of 244 peaks was significantly associated with  
331 H3K27me3 (hypergeometric test,  $p \leq 2.72^{-34}$ ). Less than half of overlapping peaks were at  
332 TSSs (Table S4). Therefore, cohesin binding significantly coincides with histone marks that  
333 are associated with active chromatin at ZGA.

334

335 The transcription factors Nanog-like, Pou5f3 and the SoxB1 family (including  
336 sox2, sox3, sox19a and sox19b) are homologs of mammalian pluripotency factors, and are  
337 thought to act as pioneering factors in zebrafish ZGA (Lee et al., 2013; Leichsenring et al.,  
338 2013). Because Rad21 depletion delayed ZGA (Fig. 2), we were interested to know whether  
339 Rad21/cohesin binding coincides with genomic locations of these activators of early gene  
340 expression. Publically available ChIP-seq data for Nanog-like (C. Xu et al. 2012), Pou5f3  
341 and Sox2 (Leichsenring et al., 2013) was obtained (Table S4) and compared to Rad21  
342 binding at 4.5 hpf. There was a small but significant overlap between Rad21 and  
343 pluripotency factor binding sites (Table S4 and Fig. 7B-D). Regions with overlap of Rad21  
344 and pluripotency factors were enriched for developmental, chromatin assembly, and pattern  
345 specification ontologies (Fig. 7B-D). The coincidence of a subset of cohesin binding with  
346 these known transcriptional activators suggests that cohesin may be involved in regulating  
347 selected Sox2 and Pou5f3 targets.

348

#### 349 **Rad21 depletion disrupts nuclear structure and RNA Polymerase II clustering at ZGA**

350 The combined data above point to a generalized role for Rad21 in early zygotic transcription.  
351 Given the known role of cohesin in the local spatial organization of chromatin  
352 (Merkenschlager and Nora, 2016), we addressed the possibility that Rad21/cohesin might  
353 contribute to ZGA through global organization of chromatin architecture.

354

355 We used antibodies to Nucleolin and RNAPII to visualize nucleoli and RNAPII clustering,  
356 respectively, immediately post-ZGA. Immunofluorescence analysis in 4.5 hpf 'dome' stage  
357 embryos revealed the formation of nucleoli (Fig. 8A,A') and discrete RNAPII clusters that  
358 may represent transcription foci (Fig. 8D,D'). Strikingly, depletion of Rad21 severely and  
359 significantly disrupted the formation of nucleoli (Fig. 8B,B',C -  $p \leq 4.7^{-14}$ ) and RNAPII clusters  
360 (Fig. 8E,E',F -  $p \leq 8.8^{-7}$ ) at this developmental stage, with these markers exhibiting a more  
361 fragmented appearance.

362

363 Ribosomal DNA (rDNA) is contained within the nucleolus and active rDNA interacts with  
364 Nucleolin (Cong et al. 2012a). In support of a direct role for Rad21 in nucleolar organization,  
365 we found that Rad21 is enriched near 5S ribosomal DNA repeats (Cong et al. 2012b) on  
366 chromosomes 4 (Fig. 5C), 18 and 22 (Table S3).

367

368 Thus, depletion of Rad21 dramatically affects nuclear organization by the time of ZGA. Our  
369 results further suggest that Rad21 recruitment to genes at this crucial developmental stage  
370 influences the formation of RNAPII foci that could represent early sites of transcription.

371 Transcripts from many genes are affected by Rad21 depletion in a manner consistent with  
372 an overall delay in ZGA (Figs 2, 3), although few of these genes are directly bound by Rad21  
373 (Fig. 6). Global disruption of chromosome organization by Rad21 depletion provides a  
374 possible mechanism for this observation.

375

376

## 377 **Discussion**

378

379 Altogether, our results point to a global role for Rad21/cohesin in facilitating ZGA in zebrafish  
380 embryos. Rad21 locates to active regions of the genome, including genes expressed at  
381 ZGA, while Rad21 depletion interferes with gene expression. Rad21 depletion also affects  
382 nuclear integrity and RNAPII clusters, raising the possibility that cohesin plays a role in  
383 organizing a chromatin structure that is permissive for transcription around the time of ZGA.

384

### 385 **Transcriptional changes at ZGA following Rad21 or CTCF depletion**

386 Owing to their important combinatorial roles in genome organization (Vietri Rudan and  
387 Hadjur, 2015), we expected Rad21/cohesin and CTCF depletion to have similar effects on  
388 activation of the zygotic genome. We were surprised to find that, upon depletion, their effects

389 were quite different. We previously showed that a modest depletion of Rad21 by morpholino  
390 (Schuster et al., 2015) or mutation (Horsfield et al., 2007) can have striking effects on the  
391 transcription of specific genes. By contrast, CTCF had to be dramatically depleted to affect  
392 transcription, and doing so resulted in high levels of mortality (data not shown and Marsman  
393 et al., 2014). CTCF is essential to the integrity of the nucleus; our data suggest that a small  
394 amount of CTCF may be sufficient for this function, and that CTCF depletion beyond this  
395 level is lethal in embryos in which cells proliferate rapidly. Consistent with this, maternal and  
396 zygotic depletion of CTCF leads to apoptosis and is lethal at preimplantation stages in mice  
397 (Moore et al., 2012; Wan et al., 2008). In contrast to CTCF, partial Rad21 depletion  
398 generated multiple robust biological effects at zebrafish ZGA, and this tractability  
399 encouraged us to focus our study on Rad21/cohesin.

400

#### 401 **Rad21 depletion delayed ZGA and dysregulated transcripts in distinct pathways**

402 Rad21 depletion dramatically altered the transcript complement in embryos just post-ZGA,  
403 reflecting an overall delay in transition from the maternal to zygotic transcription program.  
404 Among the top downregulated gene ontology categories were ribosome assembly, RNA  
405 processing and translation. These processes are also compromised by disrupting cohesin  
406 function in yeast and mammalian cells (Bose et al., 2012). Xu *et al.* previously demonstrated  
407 that translational defects in zebrafish and mammalian cell cohesin mutants were chemically  
408 rescued by L-Leucine stimulation of the TOR pathway (Xu et al., 2016; Xu et al., 2015). Our  
409 data are consistent with these observations that translational mechanisms require normal  
410 cohesin function. Moreover, cell proliferation dominates early zebrafish development and  
411 requires high levels of translation, consistent with the emergence of these biological  
412 pathways as the most significantly affected by cohesin depletion just post-ZGA.  
413 Compromising this aspect of the normal gene expression program will almost certainly affect  
414 embryogenesis, consistent with mutations in cohesin causing the human developmental  
415 disorder, Cornelia de Lange Syndrome (CdLS).



416

417 Although cell proliferation is central to early development, in *Drosophila* and zebrafish, ZGA  
418 is independent of, or upstream of cell cycle number and checkpoint regulators (Blythe and  
419 Wieschaus, 2015; Zhang et al., 2014a; Zhang et al., 2017). Consistent with these  
420 observations, we found that delay in ZGA occurred in Rad21-depleted embryos that had the  
421 same number of cells as controls. However in zebrafish, ZGA does reflect replication timing  
422 in the early embryo (Siefert et al., 2017), and we cannot rule out the possibility that  
423 replication timing is affected in our experiments.

424

#### 425 **Cohesin binding is restricted to select transcript-encoding locations pre-ZGA**

426 Rad21 was generally excluded from genes pre-ZGA with some notable exceptions. Genes  
427 that recruited Rad21 pre-ZGA included *hsp70l*, *sox2*, *gata2a*, and the *miR-430* complex. Of  
428 these, *gata2a* and *miR-430* are expressed pre-ZGA (Heyn et al., 2014), and cohesin binding  
429 to these locations was reduced once embryos transited through ZGA. Interestingly, miR-430  
430 is responsible for targeting maternal transcripts for clearance (Bazzini et al., 2012; Giraldez  
431 et al., 2006), and this raises the possibility that a proportion of maternal transcripts with  
432 delayed degradation upon Rad21 depletion could be accounted for by dysregulated *miR-*  
433 *430*.

434

435 Other genes that recruit Rad21 pre-ZGA are generally not expressed at that time. For  
436 example, *sox2* mRNA is maternally provided, and is involved in transcription of early-  
437 expressed zygotic genes in zebrafish (Lee et al., 2013). The zygotic *sox2* gene is expressed  
438 post-ZGA (Heyn et al., 2014). Significantly, the timing of *sox2* expression post-ZGA  
439 coincides with a redistribution of Rad21 peaks at the *sox2* gene. In addition, Rad21 is  
440 recruited to several zinc finger protein-encoding genes pre-ZGA that are expressed at post-  
441 ZGA stages of development. Recruitment of Rad21 to silent loci pre-ZGA could indicate that  
442 cohesin has a function there, perhaps to mark their later expression.

443

444 **Cohesin is enriched at pericentromeric satellite DNA repeats**

445 Prior to ZGA, cohesin is highly enriched at satellite DNAs found at pericentromeric regions,  
446 which represent less than 1% of the genome, as well as ncRNA genes. Various satellite  
447 sequences in somatic cells are packaged into constitutive heterochromatin, which is  
448 characterized by high compaction, enrichment of repressive histone modifications,  
449 transcriptional quiescence, and late replication. Most of these attributes are absent in pre-  
450 ZGA embryos, and the satellite sequences seem to take on these features successively as  
451 the embryo develops (Borsos and Torres-Padilla 2016). ATAC-seq indicates that the satellite  
452 DNAs are highly accessible pre-ZGA. It is possible that cohesin is sequestered there merely  
453 because this chromatin is open, and thus satellite DNA serves to keep cohesin away from  
454 RNAPII genes prior to genome activation. Cohesin depletion results in organizational  
455 changes of nucleoli, which could interfere with satellite-dependent heterochromatin formation  
456 at ZGA.

457

458 **How does cohesin contribute to transcription of the zygotic genome?**

459 At post-ZGA stages, thousands of genomic locations recruit Rad21, and markedly include  
460 genic features such as promoters, TSSs, termination sites, 3' and 5' UTRs and exons.  
461 Subsequently, Rad21 is increasingly enriched TSSs, notably at sites co-enriched in histone  
462 modifications indicative of active promoters and enhancers (Vastenhouw and Schier, 2012;  
463 Vastenhouw et al., 2010). Gene-associated Rad21 significantly overlapped with occupancy  
464 of the pluripotency factors Pou5f3 and Sox2 at similar time points. This raises the possibility  
465 that the pluripotency factors pioneer sites of zygotic transcription (Lee et al., 2013) and  
466 recruit cohesin at a subset of these to keep these regions in an 'open' configuration. In  
467 support of this idea, nucleosome density increases following cohesin loss (Yan et al., 2013),  
468 suggesting that cohesin acts to keep chromatin open. Moreover, nucleosome organization is

469 a key feature of ZGA; in zebrafish, nucleosomes are strongly positioned at promoters (Zhang  
470 et al., 2014b) at a stage that is coincident with cohesin binding.

471

472 Cohesin may also operate at a nuclear structural level to regulate ZGA. Consistent with  
473 previous observations in yeast and human cells (Bose et al., 2012; Harris et al., 2014),  
474 Rad21/cohesin is essential for the formation of nucleoli in post-ZGA zebrafish embryos. Loss  
475 of nucleoli could have global effects on zygotic transcription and translation, as was  
476 observed in this study and others (Xu et al., 2015). In addition, reduction in Rad21 just post-  
477 ZGA resulted in dispersion of RNAPII foci that could represent transcription factories. Loss of  
478 chromosome architecture owing to cohesin depletion could lead to an inability to assemble a  
479 transcription-competent genome structure.

480

481 A combination of the factors described above could lead to global dysregulation of the  
482 zygotic transcription program, and these factors are indicative of roles for cohesin at multiple  
483 levels at ZGA (Fig. 9).

484

485 A spectrum of multifactorial human developmental disorders known as the ‘cohesinopathies’  
486 arise from mutations in cohesin regulators or cohesin subunits (Ball et al., 2014; Bose and  
487 Gerton, 2010; Horsfield et al., 2012; Skibbens et al., 2013). Our study raises the possibility  
488 that germline cohesinopathy mutations could lead to global alteration of the zygotic  
489 transcription program right from the start of development, perhaps explaining the diversity of  
490 phenotypes observed in cohesinopathy patients.

491

492

493

494 **Materials and Methods**

495

496 **Zebrafish and microinjection**

497 Zebrafish were maintained under standard conditions (Westerfield, 1995). The University of  
498 Otago Animal Ethics Committee approved all zebrafish research. Morpholino  
499 oligonucleotides (MOs) were obtained from GeneTools LLC and diluted in water. MO  
500 sequences were Rad21 5'-AGGACGAAGTGGGCGTAAAACATTG-3'; and CTCF 5'-  
501 CATGGGTAATACCTACATTGGTTAA-3' (targeting the ATG), 5'-  
502 CCAAAACAGATCACAAACCTGAAAG-3' (targeting the splice site of intron 2); and Smc3 5'-  
503 TGTACATGGCGGTTTATGC-3' (targeting the ATG) as described previously (Marsman et  
504 al., 2014; Rhodes et al., 2010; Schuster et al., 2015). For microinjection, 1 nl containing 1.0  
505 pmol (for embryos up to MZT) or 0.25-0.5 pmol (for embryos grown post-MZT) of each MO  
506 was injected at the 1-cell stage. CTCF MOs were combined in an equimolar ratio. For mRNA  
507 rescue of the Rad21 MO, embryos were injected with MO from one needle and rescue  
508 mRNA (200 pg) from a second needle. Mutant *rad21<sup>nz171</sup>* mRNA (Horsfield et al., 2007) was  
509 used a control.

510

511 **RNA extraction**

512 Wild-type embryos were collected at the one-cell stage, synchronized and either morpholino-  
513 injected or kept as control and allowed to develop to the desired stage (2.5, 3.3, 4.5, 5.3, 10  
514 hpf) at 28 °C. Three biological replicates each containing total RNA from 100 pooled  
515 embryos were isolated using the NucleoSpin® RNAII Kit (Macherey-Nagel). The quality of  
516 the RNA was confirmed using the Agilent 2100 Bioanalyzer, all samples had RIN >9.

517

518 **RNA sequencing, read mapping and bioinformatics analysis**

519 Triplicate RNA samples from morphologically stage-matched embryos were sequenced to  
520 compare expression profiles over time. Strand-specific libraries were prepared using the

521 TruSeq stranded total RNA-ribozero kit (Illumina) and 100-bp paired-end sequencing was  
522 performed to depth of 10 million reads per library on an Illumina HiSeq 2000. On average, 19  
523 million 100 bp paired-end reads per library were generated. These were then adapter and  
524 quality trimmed using cutadapt (Martin, 2011) and SolexaQA (Cox et al., 2010). Each  
525 sequencing data set was independently mapped to the zebrafish genome with a bowtie2  
526 index generated from Danio\_rerio.Zv9.70 (Ensembl) downloaded from Illumina's iGenomes  
527 collection. Zebrafish genome danRer7[Zv9] was used to provide known transcript  
528 annotations from Ensembl using TopHat2 (version 2.0.9) (Kim et al., 2013) with the following  
529 options: "tophat2 --GTF genes.gtf --library-type fr-firststrand -p 24 --mate-inner-dist -8 --  
530 mate-std-dev 6 zv9" (on average, 75.38% reads mapped uniquely to the genome).  
531 Transcriptomes were assembled with Cufflinks (version 2.2.0) (Trapnell et al., 2010) using  
532 options: 'cufflinks -p 32 --GTF genes.gtf' and differential expression analysis between control  
533 and knockdown embryos was performed using Cuffdiff. A FDR corrected  $p$ -value of 0.05 was  
534 applied as the cut-off to identify differentially regulated transcripts. The R package DESeq2  
535 was used to compare expression profiles over time. The R package clusterProfiler (Yu et al.,  
536 2012) was used to identify enriched Gene ontology terms in up-regulated and down-  
537 regulated gene lists using a cut-off of 0.05 FDR corrected  $p$ -value.

538

### 539 **Quantitative PCR**

540 From RNA-seq data, five candidate genes were selected for confirmation by quantitative  
541 PCR following Rad21 and Smc3 depletion. Embryos were collected at four stages (2.5, 3.3,  
542 4.5 and 5.3 hpf), RNA extracted as above, and cDNA synthesized (qScript). Quantitative RT-  
543 PCR was performed with primers designed to each of the five candidates (Table S5).  
544 Primers were designed to span exon-exon junctions to amplify only processed mRNA  
545 transcripts. Expression was normalized to the mitochondrial gene *nd3* (Table S5).

546

547

## 548 **Antibodies**

549 Anti-Rad21 (Rhodes et al., 2010) and anti-CTCF (Marsman et al., 2014) were raised in  
550 rabbit against a 15 amino acid peptide of each of the zebrafish proteins, GenScript  
551 Corporation, USA. Commercial primary antibodies were: mouse anti- $\gamma$ -tubulin (T5326;  
552 Sigma-Aldrich), anti-nucleolin (ab22758), anti-RNA polymerase II CTD repeat YSPTSPS  
553 (phospho S2) (ab5095) (Abcam), anti-SMC3 (D47B5) rabbit mAb #5696  
554 (Cell Signaling). Secondary antibodies were: goat anti-Rabbit IgG (H+L) (#A-11008, Thermo  
555 Fisher Scientific), IRDye®-conjugated antibodies (#926-68070 and #926-32211, LiCor).

556

## 557 **Immunoblot analysis**

558 Following dechoriation and deyolking, zebrafish embryos were lysed in RIPA buffer and  
559 equal amounts of protein were separated by electrophoresis on 10% polyacrylamide gels.  
560 Proteins were transferred to nitrocellulose (Thermoscientific) and incubated with mouse anti-  
561  $\gamma$ -tubulin (1:5000) and rabbit anti-rad21 (1:500), secondary antibodies were the IRDye®-  
562 conjugated antibodies (1:15,000). Blots were visualized with the Odyssey® CLx Infrared  
563 imaging system (LiCor). Band intensities were quantified using Image Studio 4.0 Software  
564 (LiCor).

565

## 566 **Chromatin immunoprecipitation (ChIP) sequencing and analysis**

567 Chromatin was prepared from two independent collections of pooled embryos (n=2000) for  
568 2.5 hpf stage embryos and (n=1000) for 4.5 hpf and 10 hpf embryos as described in  
569 (Lindeman et al., 2009). Briefly, embryos were dechorionated using a syringe with a 21G  
570 needle, fixed in 1% formaldehyde 10 minutes at room temperature. Fixation was stopped by  
571 adding glycine to a final concentration to 0.125 M and incubation on ice for 5 minutes. Fixed  
572 embryos were then washed three times in ice cold 1x PBS, snap frozen and stored at -80 °C  
573 until use. After cell lysis, chromatin was sheared to 200-500 base pairs using a  
574 S220 Focused-ultrasonicator (Covaris) with the following settings per cycle: peak power =

575 70, duty factor = 5, cycles of bursts = 200, time=30 s. Individual cycle numbers were  
576 optimized for each stage. Chromatin from pre-MZT embryos needed 6 cycles of sonication  
577 to reach the desired 200-500 bp range, whereas chromatin isolated from 4.5 hpf and 10 hpf  
578 stages required 10 cycles. Cell debris was removed by centrifugation. To provide  
579 standardized input for each ChIP experiment, chromatin was diluted to  $A_{260}=0.25$ . For each  
580 ChIP, 6  $\mu\text{g}$  of Rad21 antibody per 10  $\mu\text{l}$  Dynabeads and 100  $\mu\text{l}$  chromatin was incubated  
581 overnight at 4 °C. After elution, ChIP DNA and input controls were purified and precipitated  
582 with ethanol.

583

584 The ThruPLEX® DNA-seq Kit (Rubicon Genomics, USA) was used to prepare the 2.5 hpf  
585 sample libraries for sequencing. 125-bp paired-end sequencing was performed to a depth of  
586 20-50 million reads per library on an Illumina HiSeq 2500™ by New Zealand Genomics  
587 Limited, NZ. Libraries for the 4.5 hpf and 10 hpf samples were constructed and sequenced  
588 at the Beijing Genomics Institute (China), yielding 20 million 50 bp single-end reads per  
589 sample. After adapter and quality trimmed using cutadapt (Martin, 2011) and SolexaQA (Cox  
590 et al., 2010), reads were aligned to the Zv9 genome assembly using bowtie2 (Langmead  
591 and Salzberg, 2012) (version 2.2.1.) with default settings. 85% of the raw reads could be  
592 aligned except for Rad21 ChIP samples from 2.5 hpf, which had a 40% mapping rate. As an  
593 alternative to bowtie2, we used the aligner SHRiMP2 (David et al., 2011), increasing the  
594 mapping rate to 79% for the 2.5 hpf Rad21 IP samples. Peak finding and downstream data  
595 analysis was performed using HOMER (Nagy et al., 2013) and MACS2 (Zhang et al., 2008).  
596 Peaks were defined at a 0.1% estimated false discovery rate. Repetitive elements were  
597 obtained from the Repeatmasker database (Tarailo-Graovac and Chen, 2009) and  
598 overlapped with Rad21 peaks using Bedtools2 (Quinlan and Hall, 2010). Heat maps were  
599 generated using the  $\log_2$  ratios of the binned reads comparing ChIP input and IP samples  
600 using deepTools2 (Galaxy version 2.2.3.0) bamCompare (Galaxy version 2.2.3),

601 computeMatrix (Galaxy version 2.2.5) and plotHeatmap (Galaxy version 2.2.5) (Ramirez et  
602 al., 2016).

603

#### 604 **Preparation and sequencing of ATAC-seq libraries**

605 The ATAC-seq libraries from zebrafish embryos were prepared as previously described  
606 (Buenrostro et al., 2015) with some modification. Embryos were collected at the 256-cell  
607 stage and dechorionated using pronase. Yolk was removed using deysolking buffer as  
608 previously described (Link et al., 2006). 75,000 cells were used to prepare the libraries.  
609 Libraries were pooled and sequenced on an Illumina HiSeq. Data was aligned to Zv9 using  
610 bowtie2 and peaks for each replicate were called using MACS2 (Zhang et al., 2008). Peaks  
611 identified in both replicates were used for downstream analysis.

612

#### 613 **Flow Cytometry**

614 Around 100 embryos at 4.5 hpf (WT and MO injected) were dechorionated and deysolking.  
615 Cells were fixed with 100% ethanol overnight. Fxycycle™ PI/RNase staining solution (Thermo  
616 Fisher Scientific) was used to stain DNA in cells. Flow cytometric acquisitions were  
617 performed on a FACSCALIBUR (BD). Analyses were performed using FlowJo software  
618 (Treestar).

619

#### 620 **Whole mount immunofluorescence**

621 Embryos were fixed, dehydrated, and stored in 100% methanol at -20 °C. For staining,  
622 embryos were rehydrated in methanol/PBT, incubated in 150 mM Tris-HCl pH 9, followed by  
623 heating at 70 °C for 15 min (Inoue and Wittbrodt, 2011). Embryos were washed and blocked  
624 in 5% sheep serum, 2 mg/ml BSA in PBT. Primary antibodies were used at 1:1000, and the  
625 secondary antibody at 1:1000 dilution together with 1:1000 Hoechst stain (Thermo Fisher  
626 Scientific) in blocking buffer. Embryos were washed in PBT and stored in DAKO mounting  
627 media until image acquisition. Confocal immunofluorescence images were acquired with a



628 confocal microscope (Nikon C2, Nikon) using a CFI Plan Fluor NA 0.3/10x objective and a  
629 NA 1.4/60x oil immersion objective.

630

### 631 **Image quantitation**

632 The Imaris software package with default parameters was used to quantify numbers of  
633 nuclei per embryo from z-stacks of Hoechst stained embryos. For quantifying nucleolar  
634 integrity and RNAPII foci, a single focal plane was obtained through the center of the  
635 nucleus. To quantify the area of immunodetected Nucleolin or RNAPII relative to the size of  
636 the nucleus, a constant threshold setting in NIS-elements imaging software (Nikon) was  
637 used for wild type and Rad21-depleted embryos. The area of the nucleus outlined by the  
638 Hoechst staining defined regions of interest for which the pixel area of Nucleolin or RNAPII  
639 was measured.

640

### 641 **Statistical analysis**

642 Statistical tests were performed using R (R Foundation for Statistical Computing, 2015).

643

### 644 **Data deposition**

645 All datasets can be found at the Gene Expression Omnibus (GEO) GSE84602.

646

### 647 **Acknowledgments**

648 The authors would like to thank Dale Dorsett for advice on ChIP-seq analysis, and Noel  
649 Jhinku for expert management of the zebrafish facility. This research was funded by Royal  
650 Society of NZ Marsden Fund [grant numbers 11-UOO-027, 16-UOO-072 to JAH], and  
651 Gravidia National Center for Growth and Development [Doctoral Scholarship to MM].

652

653 **References**

654

- 655 **Amodeo, A. A., Jukam, D., Straight, A. F. and Skotheim, J. M.** (2015). Histone titration  
656 against the genome sets the DNA-to-cytoplasm threshold for the *Xenopus* midblastula  
657 transition. *Proc Natl Acad Sci U S A* **112**, E1086-1095.
- 658 **Andersen, I. S., Lindeman, L. C., Reiner, A. H., Ostrup, O., Aanes, H., Alestrom, P. and**  
659 **Collas, P.** (2013). Epigenetic marking of the zebrafish developmental program. *Curr*  
660 *Top Dev Biol* **104**, 85-112.
- 661 **Ball, A. R., Jr., Chen, Y. Y. and Yokomori, K.** (2014). Mechanisms of cohesin-mediated  
662 gene regulation and lessons learned from cohesinopathies. *Biochim Biophys Acta*  
663 **1839**, 191-202.
- 664 **Bazzini, A. A., Lee, M. T. and Giraldez, A. J.** (2012). Ribosome profiling shows that miR-  
665 430 reduces translation before causing mRNA decay in zebrafish. *Science* **336**, 233-  
666 237.
- 667 **Blythe, S. A. and Wieschaus, E. F.** (2015). Zygotic genome activation triggers the DNA  
668 replication checkpoint at the midblastula transition. *Cell* **160**, 1169-1181.
- 669 **Bogdanovic, O., Fernandez-Minan, A., Tena, J. J., de la Calle-Mustienes, E., Hidalgo,**  
670 **C., van Kruysbergen, I., van Heeringen, S. J., Veenstra, G. J. and Gomez-**  
671 **Skarmeta, J. L.** (2012). Dynamics of enhancer chromatin signatures mark the  
672 transition from pluripotency to cell specification during embryogenesis. *Genome Res*  
673 **22**, 2043-2053.
- 674 **Bose, T. and Gerton, J. L.** (2010). Cohesinopathies, gene expression, and chromatin  
675 organization. *J Cell Biol* **189**, 201-210.
- 676 **Bose, T., Lee, K. K., Lu, S., Xu, B., Harris, B., Slaughter, B., Unruh, J., Garrett, A.,**  
677 **McDowell, W., Box, A., et al.** (2012). Cohesin proteins promote ribosomal RNA  
678 production and protein translation in yeast and human cells. *PLoS Genet* **8**, e1002749.
- 679 **Buenrostro, J. D., Wu, B., Chang, H. Y. and Greenleaf, W. J.** (2015). ATAC-seq: A  
680 Method for Assaying Chromatin Accessibility Genome-Wide. *Curr Protoc Mol Biol*  
681 **109**, 21.29.21-29.
- 682 **Cox, M. P., Peterson, D. A. and Biggs, P. J.** (2010). SolexaQA: At-a-glance quality  
683 assessment of Illumina second-generation sequencing data. *BMC Bioinformatics* **11**,  
684 485.
- 685 **David, M., Dzamba, M., Lister, D., Ilie, L. and Brudno, M.** (2011). SHRiMP2: sensitive  
686 yet practical SHort Read Mapping. *Bioinformatics* **27**, 1011-1012.
- 687 **De Iaco, A., Planet, E., Coluccio, A., Verp, S., Duc, J. and Trono, D.** (2017). DUX-family  
688 transcription factors regulate zygotic genome activation in placental mammals. *Nat*  
689 *Genet* **49**, 941-945.
- 690 **de Wit, E., Bouwman, B. A., Zhu, Y., Klous, P., Splinter, E., Verstegen, M. J., Krijger,**  
691 **P. H., Festuccia, N., Nora, E. P., Welling, M., et al.** (2013). The pluripotent genome  
692 in three dimensions is shaped around pluripotency factors. *Nature* **501**, 227-231.
- 693 **Despic, V., Dejung, M., Gu, M., Krishnan, J., Zhang, J., Herzog, L., Straube, K.,**  
694 **Gerstein, M. B., Butter, F. and Neugebauer, K. M.** (2017). Dynamic RNA-protein  
695 interactions underlie the zebrafish maternal-to-zygotic transition. *Genome Res* **27**,  
696 1184-1194.
- 697 **Fassnacht, C. and Ciosk, R.** (2017). Cell Fate Maintenance and Reprogramming During the  
698 Oocyte-to-Embryo Transition. *Results Probl Cell Differ* **59**, 269-286.

- 699 **Ferraiuolo, M. A., Rousseau, M., Miyamoto, C., Shenker, S., Wang, X. Q., Nadler, M.,**  
700 **Blanchette, M. and Dostie, J.** (2010). The three-dimensional architecture of Hox  
701 cluster silencing. *Nucleic Acids Res* **38**, 7472-7484.
- 702 **Flyamer, I. M., Gassler, J., Imakaev, M., Brandao, H. B., Ulianov, S. V., Abdennur, N.,**  
703 **Razin, S. V., Mirny, L. A. and Tachibana-Konwalski, K.** (2017). Single-nucleus  
704 Hi-C reveals unique chromatin reorganization at oocyte-to-zygote transition. *Nature*  
705 **544**, 110-114.
- 706 **Giorgetti, L., Galupa, R., Nora, E. P., Piolot, T., Lam, F., Dekker, J., Tian, G. and**  
707 **Heard, E.** (2014). Predictive polymer modeling reveals coupled fluctuations in  
708 chromosome conformation and transcription. *Cell* **157**, 950-963.
- 709 **Giraldez, A. J., Mishima, Y., Rihel, J., Grocock, R. J., Van Dongen, S., Inoue, K.,**  
710 **Enright, A. J. and Schier, A. F.** (2006). Zebrafish MiR-430 promotes deadenylation  
711 and clearance of maternal mRNAs. *Science* **312**, 75-79.
- 712 **Harris, B., Bose, T., Lee, K. K., Wang, F., Lu, S., Ross, R. T., Zhang, Y., French, S. L.,**  
713 **Beyer, A. L., Slaughter, B. D., et al.** (2014). Cohesion promotes nucleolar structure  
714 and function. *Mol Biol Cell* **25**, 337-346.
- 715 **Harrison, M. M., Li, X. Y., Kaplan, T., Botchan, M. R. and Eisen, M. B.** (2011). Zelda  
716 binding in the early *Drosophila melanogaster* embryo marks regions subsequently  
717 activated at the maternal-to-zygotic transition. *PLoS Genet* **7**, e1002266.
- 718 **Hendrickson, P. G., Dorais, J. A., Grow, E. J., Whiddon, J. L., Lim, J. W., Wike, C. L.,**  
719 **Weaver, B. D., Pflueger, C., Emery, B. R., Wilcox, A. L., et al.** (2017). Conserved  
720 roles of mouse DUX and human DUX4 in activating cleavage-stage genes and  
721 MERVL/HERVL retrotransposons. *Nat Genet* **49**, 925-934.
- 722 **Heyn, P., Kircher, M., Dahl, A., Kelso, J., Tomancak, P., Kalinka, A. T. and**  
723 **Neugebauer, K. M.** (2014). The earliest transcribed zygotic genes are short, newly  
724 evolved, and different across species. *Cell Rep* **6**, 285-292.
- 725 **Hontelez, S., van Kruijsbergen, I., Georgiou, G., van Heeringen, S. J., Bogdanovic, O.,**  
726 **Lister, R. and Veenstra, G. J.** (2015). Embryonic transcription is controlled by  
727 maternally defined chromatin state. *Nat Commun* **6**, 10148.
- 728 **Horsfield, J. A., Anagnostou, S. H., Hu, J. K., Cho, K. H., Geisler, R., Lieschke, G.,**  
729 **Crosier, K. E. and Crosier, P. S.** (2007). Cohesin-dependent regulation of Runx  
730 genes. *Development* **134**, 2639-2649.
- 731 **Horsfield, J. A., Print, C. G. and Monnich, M.** (2012). Diverse developmental disorders  
732 from the one ring: distinct molecular pathways underlie the cohesinopathies. *Front*  
733 *Genet* **3**, 171.
- 734 **Hug, C. B., Grimaldi, A. G., Kruse, K. and Vaquerizas, J. M.** (2017). Chromatin  
735 Architecture Emerges during Zygotic Genome Activation Independent of  
736 Transcription. *Cell* **169**, 216-228 e219.
- 737 **Inoue, D. and Wittbrodt, J.** (2011). One for all--a highly efficient and versatile method for  
738 fluorescent immunostaining in fish embryos. *PLoS One* **6**, e19713.
- 739 **Jevtic, P. and Levy, D. L.** (2015). Nuclear size scaling during *Xenopus* early development  
740 contributes to midblastula transition timing. *Curr Biol* **25**, 45-52.
- 741 **Jiang, L., Zhang, J., Wang, J. J., Wang, L., Zhang, L., Li, G., Yang, X., Ma, X., Sun, X.,**  
742 **Cai, J., et al.** (2013). Sperm, but not oocyte, DNA methylome is inherited by  
743 zebrafish early embryos. *Cell* **153**, 773-784.
- 744 **Joseph, S. R., Palfy, M., Hilbert, L., Kumar, M., Karschau, J., Zaburdaev, V.,**  
745 **Shevchenko, A. and Vastenhouw, N. L.** (2017). Competition between histone and  
746 transcription factor binding regulates the onset of transcription in zebrafish embryos.  
747 *Elife* **6**.

- 748 **Kim, D., Pertea, G., Trapnell, C., Pimentel, H., Kelley, R. and Salzberg, S. L.** (2013).  
749 TopHat2: accurate alignment of transcriptomes in the presence of insertions, deletions  
750 and gene fusions. *Genome Biol* **14**, R36.
- 751 **Kimelman, D., Kirschner, M. and Scherson, T.** (1987). The events of the midblastula  
752 transition in *Xenopus* are regulated by changes in the cell cycle. *Cell* **48**, 399-407.
- 753 **Krijger, P. H. and de Laat, W.** (2017). Can We Just Say: Transcription Second? *Cell* **169**,  
754 184-185.
- 755 **Langmead, B. and Salzberg, S. L.** (2012). Fast gapped-read alignment with Bowtie 2. *Nat*  
756 *Methods* **9**, 357-359.
- 757 **Lee, M. T., Bonneau, A. R., Takacs, C. M., Bazzini, A. A., DiVito, K. R., Fleming, E. S.**  
758 **and Giraldez, A. J.** (2013). Nanog, Pou5f1 and SoxB1 activate zygotic gene  
759 expression during the maternal-to-zygotic transition. *Nature* **503**, 360-364.
- 760 **Leichsenring, M., Maes, J., Mossner, R., Driever, W. and Onichtchouk, D.** (2013).  
761 Pou5f1 transcription factor controls zygotic gene activation in vertebrates. *Science*  
762 **341**, 1005-1009.
- 763 **Li, X.-Y., Harrison, M. M., Villalta, J. E., Kaplan, T. and Eisen, M. B.** (2014).  
764 *Establishment of regions of genomic activity during the Drosophila maternal to*  
765 *zygotic transition.*
- 766 **Lindeman, L. C., Andersen, I. S., Reiner, A. H., Li, N., Aanes, H., Ostrup, O., Winata,**  
767 **C., Mathavan, S., Muller, F., Alestrom, P., et al.** (2011). Prepatterning of  
768 developmental gene expression by modified histones before zygotic genome  
769 activation. *Dev Cell* **21**, 993-1004.
- 770 **Lindeman, L. C., Vogt-Kielland, L. T., Alestrom, P. and Collas, P.** (2009). Fish'n ChIPs:  
771 chromatin immunoprecipitation in the zebrafish embryo. *Methods Mol Biol* **567**, 75-  
772 86.
- 773 **Link, V., Shevchenko, A. and Heisenberg, C. P.** (2006). Proteomics of early zebrafish  
774 embryos. *BMC Dev Biol* **6**, 1.
- 775 **Lu, F., Liu, Y., Inoue, A., Suzuki, T., Zhao, K. and Zhang, Y.** (2016). Establishing  
776 Chromatin Regulatory Landscape during Mouse Preimplantation Development. *Cell*  
777 **165**, 1375-1388.
- 778 **Marco, A.** (2017). Clearance of Maternal RNAs: Not a Mummy's Embryo Anymore.  
779 *Methods Mol Biol* **1605**, 1-10.
- 780 **Marsman, J., O'Neill, A. C., Kao, B. R., Rhodes, J. M., Meier, M., Antony, J., Monnich,**  
781 **M. and Horsfield, J. A.** (2014). Cohesin and CTCF differentially regulate  
782 spatiotemporal runx1 expression during zebrafish development. *Biochim Biophys*  
783 *Acta* **1839**, 50-61.
- 784 **Martin, M.** (2011). CutAdapt removes adapter sequences from high-throughput sequencing  
785 reads. *EMBnetjournal* **17**.
- 786 **Merkenschlager, M. and Nora, E. P.** (2016). CTCF and Cohesin in Genome Folding and  
787 Transcriptional Gene Regulation. *Annu Rev Genomics Hum Genet* **17**, 17-43.
- 788 **Moore, J. M., Rabaia, N. A., Smith, L. E., Fagerlie, S., Gurley, K., Loukinov, D.,**  
789 **Disteche, C. M., Collins, S. J., Kemp, C. J., Lobanenkova, V. V., et al.** (2012). Loss  
790 of maternal CTCF is associated with peri-implantation lethality of Ctcf null embryos.  
791 *PLoS One* **7**, e34915.
- 792 **Nagy, G., Daniel, B., Jonas, D., Nagy, L. and Barta, E.** (2013). A novel method to predict  
793 regulatory regions based on histone mark landscapes in macrophages. *Immunobiology*  
794 **218**, 1416-1427.

- 795 **Narendra, V., Rocha, P. P., An, D., Raviram, R., Skok, J. A., Mazzoni, E. O. and**  
796 **Reinberg, D.** (2015). CTCF establishes discrete functional chromatin domains at the  
797 Hox clusters during differentiation. *Science* **347**, 1017-1021.
- 798 **Nasmyth, K. and Haering, C. H.** (2005). The structure and function of SMC and kleisin  
799 complexes. *Annu Rev Biochem* **74**, 595-648.
- 800 **Newman, J. J. and Young, R. A.** (2010). Connecting transcriptional control to chromosome  
801 structure and human disease. *Cold Spring Harb Symp Quant Biol* **75**, 227-235.
- 802 **Newport, J. and Kirschner, M.** (1982a). A major developmental transition in early *Xenopus*  
803 embryos: I. characterization and timing of cellular changes at the midblastula stage.  
804 *Cell* **30**, 675-686.
- 805 ---- (1982b). A major developmental transition in early *Xenopus* embryos: II. Control of the  
806 onset of transcription. *Cell* **30**, 687-696.
- 807 **Nora, E. P., Goloborodko, A., Valton, A. L., Gibcus, J. H., Uebersohn, A., Abdennur, N.,**  
808 **Dekker, J., Mirny, L. A. and Bruneau, B. G.** (2017). Targeted Degradation of  
809 CTCF Decouples Local Insulation of Chromosome Domains from Genomic  
810 Compartmentalization. *Cell* **169**, 930-944 e922.
- 811 **Nothias, J. Y., Majumder, S., Kaneko, K. J. and DePamphilis, M. L.** (1995). Regulation  
812 of gene expression at the beginning of mammalian development. *J Biol Chem* **270**,  
813 22077-22080.
- 814 **Onichtchouk, D. and Driever, W.** (2016). Zygotic Genome Activators, Developmental  
815 Timing, and Pluripotency. *Curr Top Dev Biol* **116**, 273-297.
- 816 **Palfy, M., Joseph, S. R. and Vastenhouw, N. L.** (2017). The timing of zygotic genome  
817 activation. *Curr Opin Genet Dev* **43**, 53-60.
- 818 **Phillips-Cremins, J. E.** (2014). Unraveling architecture of the pluripotent genome. *Curr*  
819 *Opin Cell Biol* **28**, 96-104.
- 820 **Potok, M. E., Nix, D. A., Parnell, T. J. and Cairns, B. R.** (2013). Reprogramming the  
821 maternal zebrafish genome after fertilization to match the paternal methylation  
822 pattern. *Cell* **153**, 759-772.
- 823 **Quinlan, A. R. and Hall, I. M.** (2010). BEDTools: a flexible suite of utilities for comparing  
824 genomic features. *Bioinformatics* **26**.
- 825 **R Foundation for Statistical Computing, V., Austria** (2015). R: A language and  
826 environment for statistical computing.
- 827 **Ramirez, F., Ryan, D. P., Gruning, B., Bhardwaj, V., Kilpert, F., Richter, A. S., Heyne,**  
828 **S., Dunder, F. and Manke, T.** (2016). deepTools2: a next generation web server for  
829 deep-sequencing data analysis. *Nucleic Acids Res* **44**, W160-165.
- 830 **Rhodes, J. M., Bentley, F. K., Print, C. G., Dorsett, D., Misulovin, Z., Dickinson, E. J.,**  
831 **Crosier, K. E., Crosier, P. S. and Horsfield, J. A.** (2010). Positive regulation of c-  
832 Myc by cohesin is direct, and evolutionarily conserved. *Dev Biol* **344**, 637-649.
- 833 **Rousseau, M., Crutchley, J. L., Miura, H., Suderman, M., Blanchette, M. and Dostie, J.**  
834 (2014). Hox in motion: tracking HoxA cluster conformation during differentiation.  
835 *Nucleic Acids Res* **42**, 1524-1540.
- 836 **Schuster, K., Leeke, B., Meier, M., Wang, Y., Newman, T., Burgess, S. and Horsfield, J.**  
837 **A.** (2015). A neural crest origin for cohesinopathy heart defects. *Hum Mol Genet* **24**,  
838 7005-7016.
- 839 **Siefert, J. C., Georgescu, C., Wren, J. D., Koren, A. and Sansam, C. L.** (2017). DNA  
840 replication timing during development anticipates transcriptional programs and  
841 parallels enhancer activation. *Genome Res* **27**, 1406-1416.

- 842 **Skibbens, R. V., Colquhoun, J. M., Green, M. J., Molnar, C. A., Sin, D. N., Sullivan, B.**  
843 **J. and Tanzosh, E. E.** (2013). Cohesinopathies of a feather flock together. *PLoS*  
844 *Genet* **9**, e1004036.
- 845 **Svoboda, P., Franke, V. and Schultz, R. M.** (2015). Chapter Nine - Sculpting the  
846 Transcriptome During the Oocyte-to-Embryo Transition in Mouse. In *Current Topics*  
847 *in Developmental Biology* (ed. D. L. Howard), pp. 305-349: Academic Press.
- 848 **Tarailo-Graovac, M. and Chen, N.** (2009). Using RepeatMasker to identify repetitive  
849 elements in genomic sequences. *Curr Protoc Bioinformatics* **Chapter 4**, Unit 4 10.
- 850 **Trapnell, C., Williams, B. A., Pertea, G., Mortazavi, A., Kwan, G., van Baren, M. J.,**  
851 **Salzberg, S. L., Wold, B. J. and Pachter, L.** (2010). Transcript assembly and  
852 quantification by RNA-Seq reveals unannotated transcripts and isoform switching  
853 during cell differentiation. *Nat Biotechnol* **28**, 511-515.
- 854 **Van Bortle, K., Nichols, M. H., Li, L., Ong, C. T., Takenaka, N., Qin, Z. S. and Corces,**  
855 **V. G.** (2014). Insulator function and topological domain border strength scale with  
856 architectural protein occupancy. *Genome Biol* **15**, R82.
- 857 **Vastenhouw, N. L. and Schier, A. F.** (2012). Bivalent histone modifications in early  
858 embryogenesis. *Curr Opin Cell Biol* **24**, 374-386.
- 859 **Vastenhouw, N. L., Zhang, Y., Woods, I. G., Imam, F., Regev, A., Liu, X. S., Rinn, J.**  
860 **and Schier, A. F.** (2010). Chromatin signature of embryonic pluripotency is  
861 established during genome activation. *Nature* **464**, 922-926.
- 862 **Vietri Rudan, M., Barrington, C., Henderson, S., Ernst, C., Odom, D. T., Tanay, A. and**  
863 **Hadjur, S.** (2015). Comparative Hi-C reveals that CTCF underlies evolution of  
864 chromosomal domain architecture. *Cell Rep* **10**, 1297-1309.
- 865 **Vietri Rudan, M. and Hadjur, S.** (2015). Genetic Tailors: CTCF and Cohesin Shape the  
866 Genome During Evolution. *Trends Genet* **31**, 651-660.
- 867 **Wan, L. B., Pan, H., Hannenhalli, S., Cheng, Y., Ma, J., Fedoriw, A., Lobanenkov, V.,**  
868 **Latham, K. E., Schultz, R. M. and Bartolomei, M. S.** (2008). Maternal depletion of  
869 CTCF reveals multiple functions during oocyte and preimplantation embryo  
870 development. *Development* **135**, 2729-2738.
- 871 **Westerfield, M.** (1995). *The Zebrafish Book. A guide for the laboratory use of zebrafish*  
872 *(Brachydanio rerio)*. Eugene, Oregon: University of Oregon Press.
- 873 **Whiddon, J. L., Langford, A. T., Wong, C. J., Zhong, J. W. and Tapscott, S. J.** (2017).  
874 Conservation and innovation in the DUX4-family gene network. *Nat Genet* **49**, 935-  
875 940.
- 876 **Xu, B., Gogol, M., Gaudenz, K. and Gerton, J. L.** (2016). Improved transcription and  
877 translation with L-leucine stimulation of mTORC1 in Roberts syndrome. *BMC*  
878 *Genomics* **17**, 25.
- 879 **Xu, B., Sowa, N., Cardenas, M. E. and Gerton, J. L.** (2015). L-leucine partially rescues  
880 translational and developmental defects associated with zebrafish models of Cornelia  
881 de Lange syndrome. *Hum Mol Genet* **24**, 1540-1555.
- 882 **Yan, J., Enge, M., Whittington, T., Dave, K., Liu, J., Sur, I., Schmierer, B., Jolma, A.,**  
883 **Kivioja, T., Taipale, M., et al.** (2013). Transcription factor binding in human cells  
884 occurs in dense clusters formed around cohesin anchor sites. *Cell* **154**, 801-813.
- 885 **Yu, G., Wang, L. G., Han, Y. and He, Q. Y.** (2012). clusterProfiler: an R package for  
886 comparing biological themes among gene clusters. *OMICS* **16**, 284-287.
- 887 **Zhang, M., Kothari, P., Mullins, M. and Lampson, M. A.** (2014a). Regulation of zygotic  
888 genome activation and DNA damage checkpoint acquisition at the mid-blastula  
889 transition. *Cell Cycle* **13**, 3828-3838.

- 890 **Zhang, M., Skirkanich, J., Lampson, M. A. and Klein, P. S.** (2017). Cell Cycle  
891 Remodeling and Zygotic Gene Activation at the Midblastula Transition. *Adv Exp Med*  
892 *Biol* **953**, 441-487.
- 893 **Zhang, Y., Liu, T., Meyer, C. A., Eeckhoute, J., Johnson, D. S., Bernstein, B. E.,**  
894 **Nusbaum, C., Myers, R. M., Brown, M., Li, W., et al.** (2008). Model-based  
895 analysis of ChIP-Seq (MACS). *Genome Biol* **9**, R137.
- 896 **Zhang, Y., Vastenhouw, N. L., Feng, J., Fu, K., Wang, C., Ge, Y., Pauli, A., van**  
897 **Hummelen, P., Schier, A. F. and Liu, X. S.** (2014b). Canonical nucleosome  
898 organization at promoters forms during genome activation. *Genome Res* **24**, 260-266.
- 899 **Zhao, B. S., Wang, X., Beadell, A. V., Lu, Z., Shi, H., Kuuspalu, A., Ho, R. K. and He,**  
900 **C.** (2017). m6A-dependent maternal mRNA clearance facilitates zebrafish maternal-  
901 to-zygotic transition. *Nature* **542**, 475-478.  
902
- 903

904 **Tables**

905

906 **Table 1. Genome wide distribution of selected repeat elements and overlap with pre-**

907 **ZGA Rad21 binding.**

908

<b>Repeat element</b>	<b>Number of elements in zv9</b>	<b>Rad21 overlap</b>	<b>p-values for fisher's exact test (right-tail)</b>	<b>Odds ratio</b>	<b>Genome wide coverage</b>
<b>LTRs</b>	153185	200	7.15E-18	2.013	4.97%
<b>DNA transposons</b>	1980516	153	1	0.143	33.88%
<b>rDNAs</b>	3628	136	1.00E-20	204.286	0.04%
<b>BRSATI</b>	235	402	1.00E-20	inf	0.10%
<b>SAT-1 DR</b>	176	396	1.00E-20	inf	0.06%
<b>MOSAT DR</b>	10546	13	0.01641	2.026	0.29%

909

910

911



912 **Figure legends**

913

914 **Figure 1. Rad21 and CTCF are present pre-ZGA and can be effectively depleted in**

915 **early zebrafish development.** (A) As embryos reach MZT, maternal transcripts are  
916 degraded and zygotic transcripts accumulate. The series of embryos below represents time  
917 points that were sampled for RNA-seq. hpf = hours post-fertilization. (B) Transcript numbers  
918 expressed as fragments per kilobase mapped (FPKM) of Rad21 and CTCF as measured by  
919 RNA-seq across the indicated time points. Error bars represent 95% confidence intervals.  
920 (C) Quantitation of immunoblots for Rad21 and CTCF protein levels, normalized against  
921 those of  $\gamma$ -tubulin. Data are means  $\pm$  s.d. n = 3. (D) Quantitation of immunoblots for Rad21  
922 and CTCF protein levels, following depletion of these proteins using morpholino  
923 oligonucleotides (Rad21 knockdown (KD) and CTCF KD). Protein levels are expressed as a  
924 percent of wild type levels and were normalized against those of  $\gamma$ -tubulin. Images of all  
925 immunoblots are provided in Figs S1, S1E.

926

927 **Figure 2. Rad21 depletion delays the onset of the zygotic transcription program.** (A)

928 PCA plot of RNA-seq triplicate samples for pools (n=100) of wild type (WT), Rad21-depleted  
929 (KD) and CTCF-depleted (KD) conditions at time points 2.5-5.3 hpf. PC1 and PC2, together  
930 accounting for 97% of the variation, identify sample separation by developmental time.  
931 Samples from different conditions (WT, Rad21 KD and CTCF KD) show clustered  
932 differences at 4.5 hpf and 5.3 hpf. (B) Number of differentially represented transcripts in  
933 Rad21 KD and CTCF KD embryos at stages 2.5-10 hpf. (C) Scatterplot of differentially  
934 represented transcripts (total = 3,253, FDR=0.05) between WT and Rad21 KD at 4.5 hpf. (D)  
935 Scatterplot of differentially represented transcripts (total = 888, FDR=0.05) between WT and  
936 CTCF KD at 4.5 hpf. Histograms depict the number of over-represented (y-axis) and under-  
937 represented transcripts (x-axis) in (C) and (D).

938

939 **Figure 3. Cohesin depletion delays expression of zygotic genes.** (A, B) Distribution of  
940 significantly differentially represented transcripts (FDR 0.05) in Rad21-depleted embryos  
941 over developmental time points (2.5-5.3 hpf). The bottom and top of the boxes represent the  
942 first and third quartiles, and the line within represents the median; notches represent  
943 confidence intervals. The whiskers denote the interval within 1.5 times the interquartile range  
944 (IQR) from the median. (A) FPKM over developmental time of 1,286 transcripts that were  
945 reduced in Rad21-depleted (KD) embryos. (B) FPKM over developmental time of 2,381  
946 transcripts with elevated levels in Rad21-depleted (KD) embryos. (C) Quantitative RT-PCR  
947 of selected zygotically-expressed transcripts that were differentially represented in RNA-seq  
948 data. Embryos were injected at the one-cell stage with 1 pmol Rad21 or Smc3 morpholino  
949 respectively, and ~50 per condition were pooled for RNA extraction. Data were normalized  
950 to mitochondrial transcript *nd3* and shown as a scatter plot with means and 95% confidence  
951 intervals (3 biological replicates per condition). *p*-values (\* <0.05, \*\* <0.01, \*\*\* <0.001  
952 unpaired *t*-test).

953

954 **Figure 4. Gene ontologies of differentially represented transcripts in Rad21-depleted**  
955 **embryos.** Enriched gene ontology (GO) terms and their binomial *p*-values with fold  
956 enrichment over expected number was derived using R package clusterProfiler to analyze  
957 differentially represented transcripts upon Rad21 depletion. (A) transcripts under-  
958 represented in Rad21-depleted embryos at 4.5 hpf; (B) transcripts over-represented in  
959 Rad21-depleted embryos at 4.5 hpf. The full list of GO terms that were enriched can be  
960 found in Table S2.

961

962 **Figure 5. Rad21 binding redistributes to coding regions during ZGA.** (A) Violin plots of  
963 the absolute distance to the TSS of Rad21-associated genes for stages 2.5, 4.5 and 10 hpf,  
964 including median values. The bottom and top of the boxes are the first and third quartiles,  
965 and the line within represents the median. The whiskers denote the interval within 1.5 times

966 the interquartile range (IQR) from the median. (B) Overlap of ATAC-seq peaks at 2.5 hpf  
967 with Rad21 distribution at 2.5 hpf. The  $p$ -value was calculated using Fisher's exact test  
968 (right-tail). (C) IGV genome browser view of chromosome 4. Rad21 locates to gene-poor  
969 regions on the long arm pre-ZGA but binds gene-rich regions on the short arm post-ZGA.  
970 Repetitive elements such as tRNAs, ribosomal RNAs (5S RNA) are highly enriched on  
971 chromosome 4 and overlap with Rad21. Satellite repeats (BRSATI and SAT-1) enriched at  
972 pericentromeric regions are also bound by Rad21 at 2.5 hpf. (red box). (D-E) Pie plots  
973 representing various repetitive elements overlapping pre-ZGA ATAC-seq peaks at 2.5 hpf  
974 (D) and Rad21 peaks only at 2.5 hpf (E). 51% (173/337) of the ATAC-seq peaks and 41%  
975 (824/2011) of the Rad21 peaks associate with satellite repeats BRSATI and SAT-1.

976

977 **Figure 6. Post-ZGA Rad21 binding is enriched at genes and overlaps with**

978 **differentially represented transcripts.** (A) Enrichment of genomic features (3' UTR, TSS,  
979 Exon, Intron, Promoter, 5' UTR) at Rad21 binding sites. (B) Overlap between Rad21-bound  
980 genes and differentially represented transcripts upon Rad21 depletion was significantly  
981 enriched at 4.5 hpf (Fisher's exact test:  $p \leq 5.39^{-20}$ , downregulated transcripts;  $p \leq 1.630^{-6}$ ,  
982 upregulated transcripts). (C, D) Heat maps showing binding profiles of Rad21 at 4.5 hpf and  
983 10 hpf, at regions associated with genes encoding over-represented transcripts (C) and  
984 under-represented transcripts (D) in 4.5 hpf Rad21-depleted embryos (KD). (E) Expression  
985 levels of genes associated with regions in (C) and (D) in 10 hpf wild type embryos. The  
986 bottom and top of the boxes are the first and third quartiles, and the line within represents  
987 the median. The whiskers denote the interval within 1.5 times the interquartile range. Rad21-  
988 bound genes with under-represented transcript levels upon Rad21 depletion (KD) at 4.5 hpf  
989 have higher FPKMs in 10 hpf wild type (WT) embryos than Rad21-bound genes with over-  
990 represented transcript levels upon Rad21 depletion at 4.5 hpf. All  $p$ -values were calculated  
991 using the Mann-Whitney-Wilcoxon test. (F) Number of differentially expressed (DE) genes in  
992 10 hpf Rad21-depleted (KD) embryos.

993

994 **Figure 7. A subset of Rad21 binding sites coincide with occupancy of active histone**  
995 **marks and pluripotency factors, Nanog-like, Pou5f3 and Sox2.** (A) Histone modifications  
996 at Rad21 binding sites. Heat maps and average profiles showing enrichment of histone  
997 marks over defined regions centered on individual Rad21 peaks at 4.5 hpf. Heat maps are  
998 ordered by decreasing enrichment for each histone modification independently. Weighted  
999 Venn diagram of Rad21 peaks overlapping with different histone modification peaks from 4.5  
1000 hpf embryos. For Rad21 overlap with histone marks, a hypergeometric test was used. (B)  
1001 Heat maps and average profiles showing enrichment of Nanog-like binding at Rad21 peaks  
1002 at 4.5 hpf. Significantly enriched gene ontologies of Rad21 and Nanog-like overlapping  
1003 regions. (C) Heat maps and average profiles showing Rad21 enrichment at Pou5f3 peaks.  
1004 Significantly enriched gene ontologies of Rad21 and Pou5f3 overlapping regions. (D) Heat  
1005 maps and average profiles showing Rad21 enrichment at Sox2 peaks. Significantly enriched  
1006 gene ontologies of Rad21- and Sox2-overlapping regions.

1007

1008 **Figure 8. Formation of sub-nuclear structures in post-ZGA embryos is compromised**  
1009 **by Rad21 depletion.** Rad21-depleted (Rad21 KD) and wild type (WT) stage-matched  
1010 control embryos at 4.5 hpf were fixed and stained with the indicated antibodies. For all  
1011 images, nuclei were counterstained with Hoescht, and the scale bar is 10  $\mu\text{m}$ . (A, A')  
1012 Nucleolin staining (green) in wild type is shown in a field of cells (A) and in a z-stack  
1013 maximum projection of a single representative nucleus (A'), and indicates the presence of  
1014 normal nucleoli. (B, B') Nucleolin staining (green) in Rad21-depleted embryos is shown in a  
1015 field of cells (B) and in a z-stack maximum projection (B'), and indicates nucleolar dispersion  
1016 following abrogation of Rad21. (C) Quantification of the area of Nucleolin relative to the size  
1017 of the nucleus in stage-matched wild type embryos compared with Rad21-depleted embryos  
1018 at 4.5 hpf (see methods; n=6 for both conditions) shows that nucleoli fragmentation is  
1019 significant. Around 200 nuclei for each condition were imaged and analyzed. (D, D') Staining

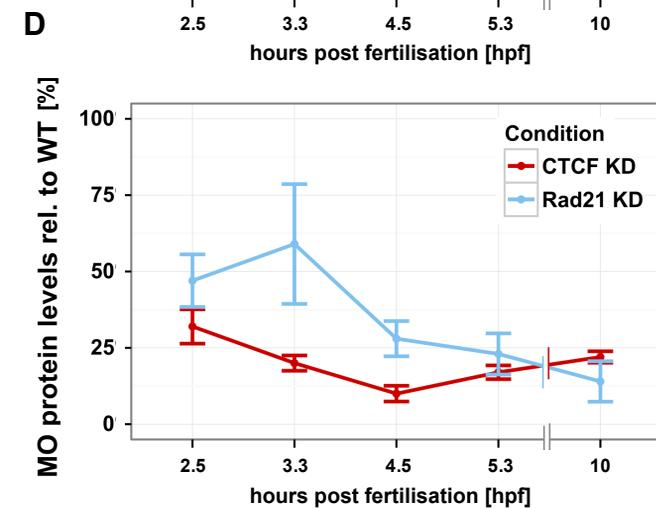
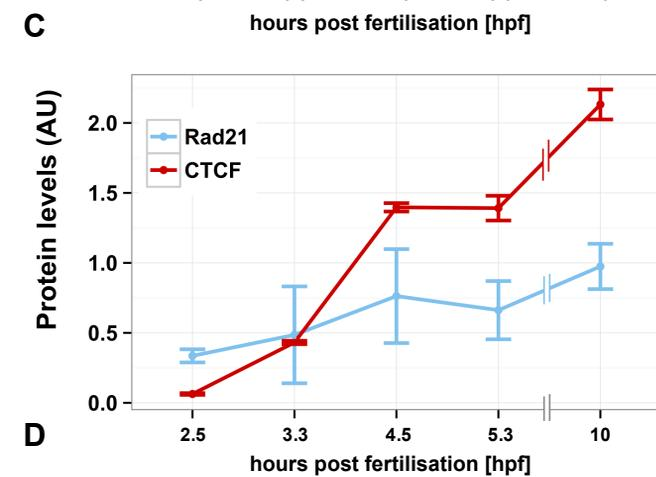
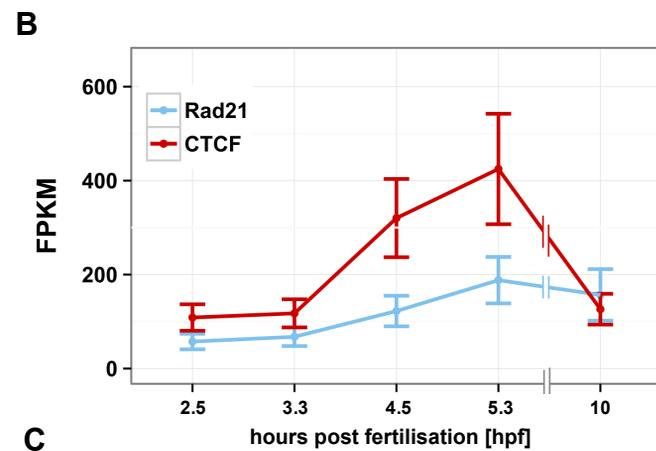
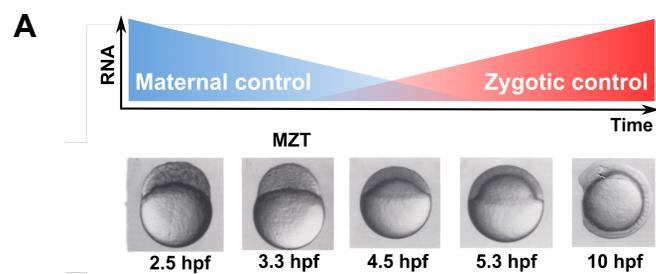
1020 for the elongating form of RNA polymerase II (p-Ser2-RNAPII) (green) in wild type is shown  
1021 in a field of cells (D) and in a z-stack maximum projection of a single representative nucleus  
1022 (D'), and indicates clustering of RNAPII into foci. (E, E') p-Ser2-RNAPII staining (green) in  
1023 Rad21-depleted 4.5 hpf embryos is shown in a field of cells (E) and in a z-stack maximum  
1024 projection (E') shows disruption of RNAPII foci upon Rad21 depletion. (F) Quantification of  
1025 RNAPII foci relative to the size of the nucleus shows statistically significant disruption of  
1026 RNAPII clustering in Rad21-depleted embryos compared with controls (see methods; n=6  
1027 for both conditions). Around 200 nuclei for each condition were imaged and analyzed. All *p*  
1028 values were calculated by applying a *t*-test with an unpaired fit and assuming a parametric  
1029 distribution.

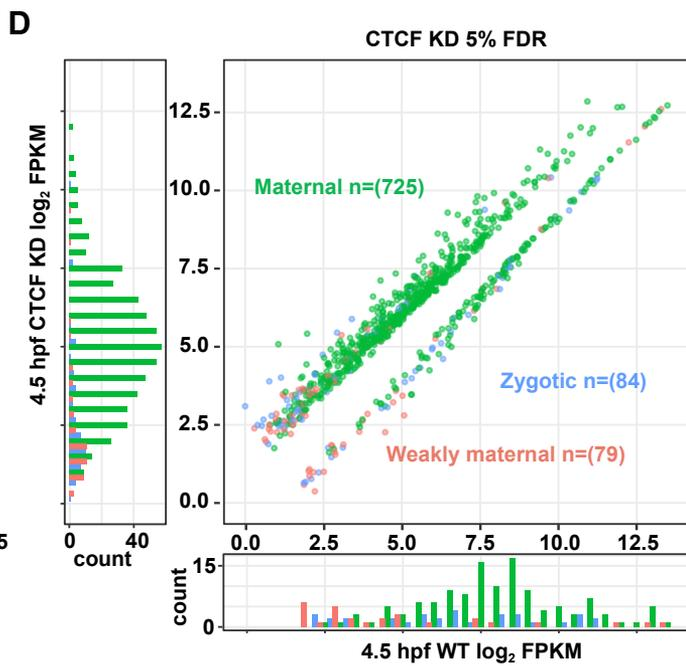
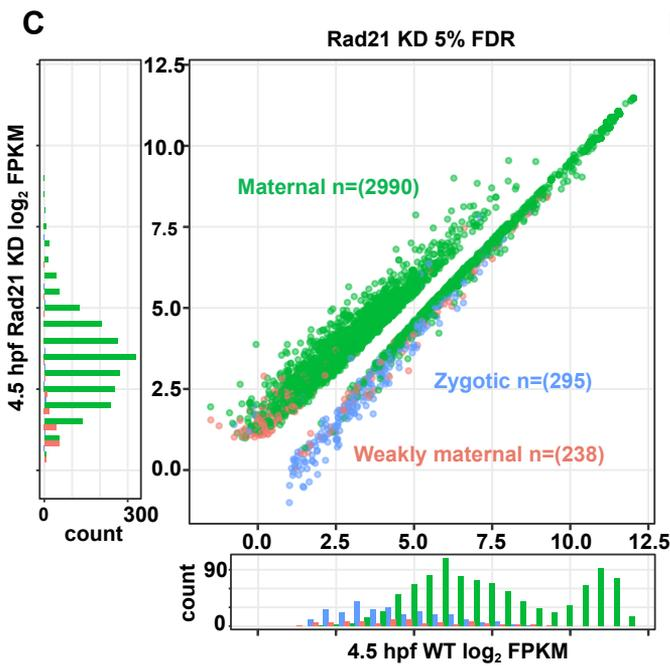
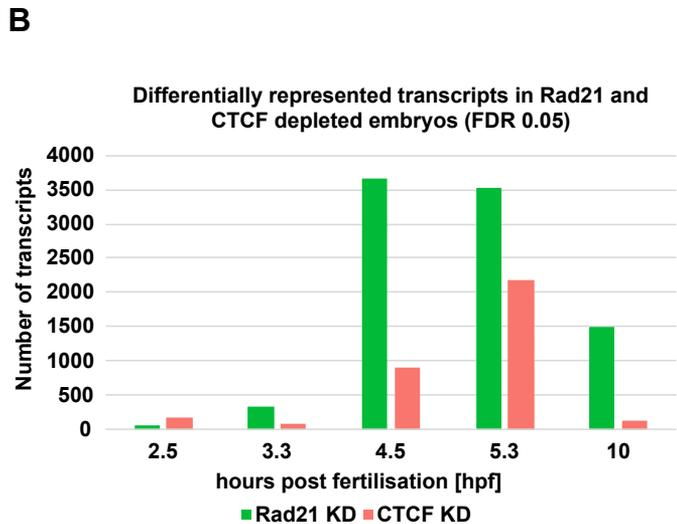
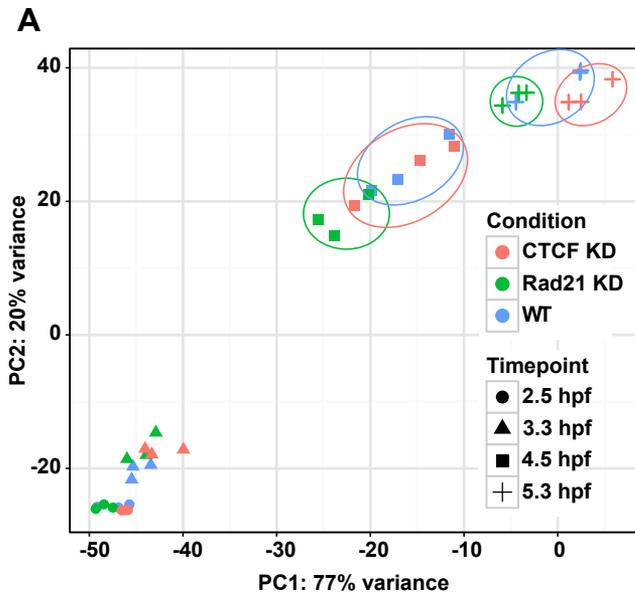
1030

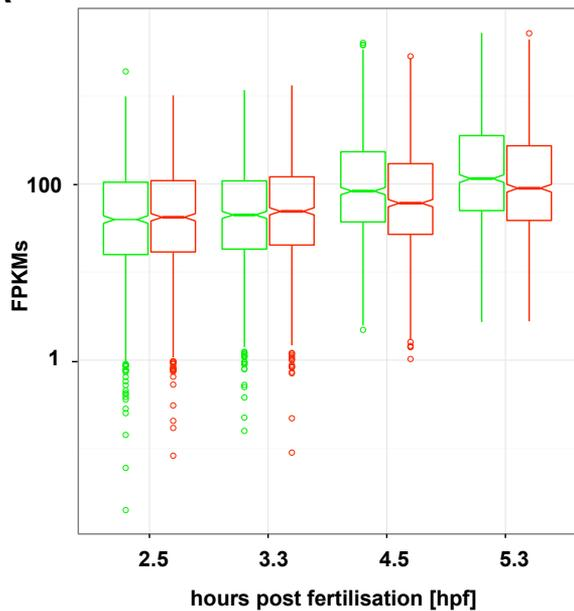
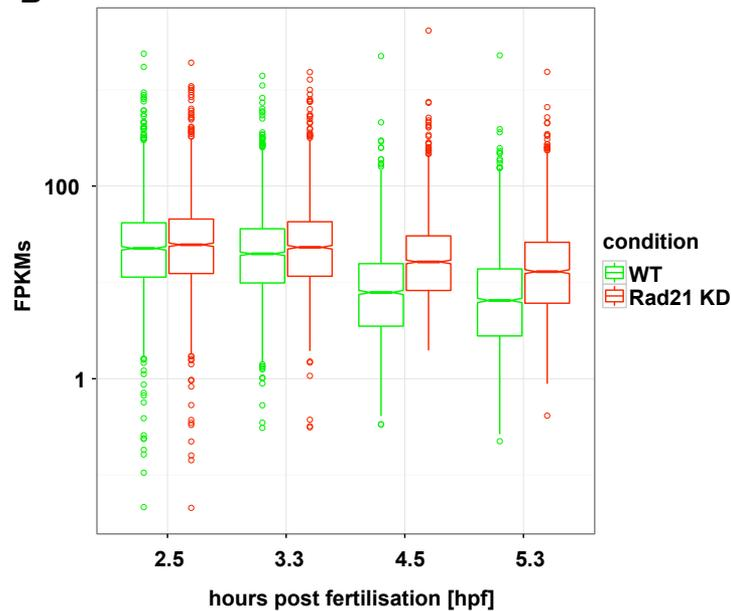
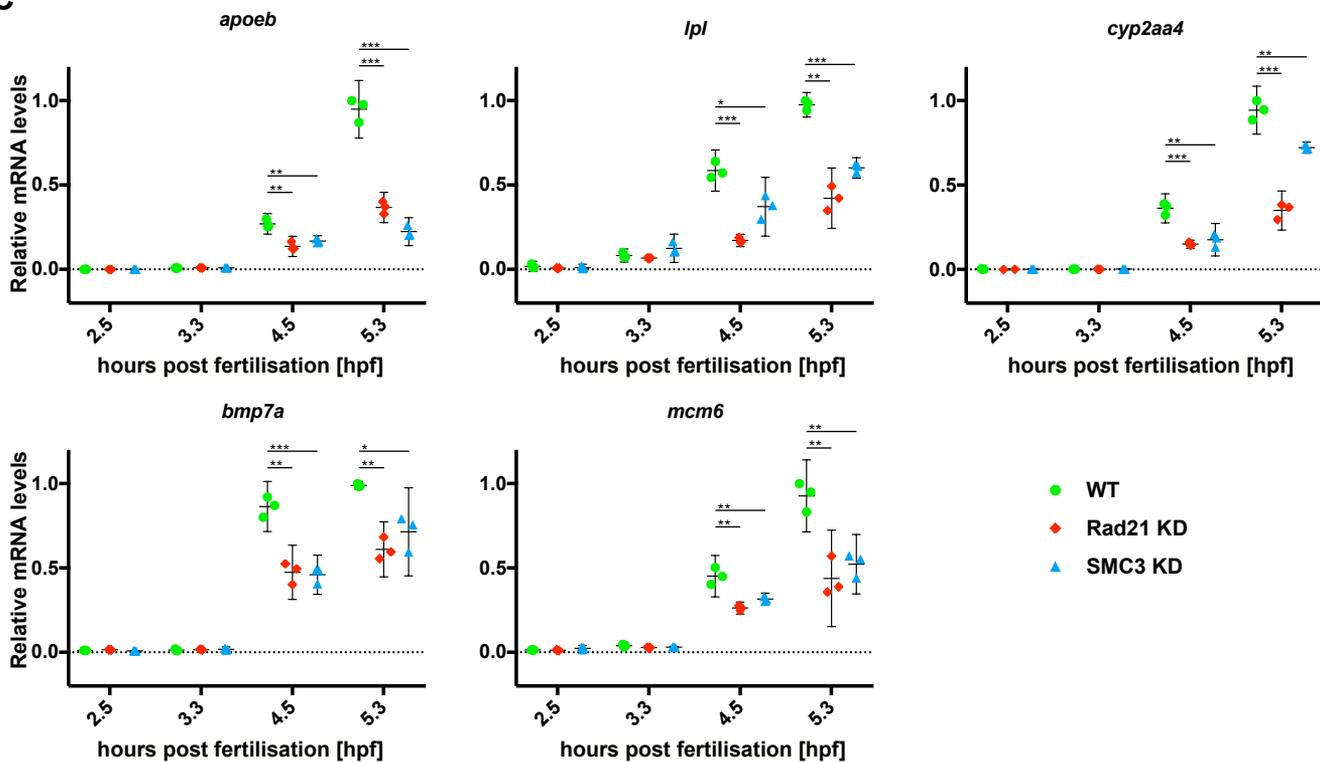
1031

1032 **Figure 9. Model of potential mechanisms for cohesin regulation at ZGA.** Up until ZGA,  
1033 cohesin locates to accessible regions of the genome, including miR-430 and satellite DNA.  
1034 As embryos transit through ZGA, cohesin relocates to RNAPII genes. Access of cohesin to  
1035 zygotic genes may be regulated by transcription factors Pou5f3, SoxB1 and Nanog.  
1036 Enrichment of cohesin at genes may contribute to forming transcription competent local and  
1037 global chromatin structures.

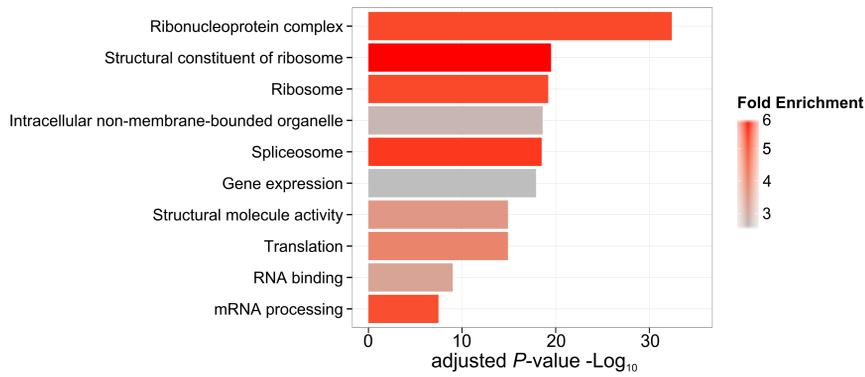
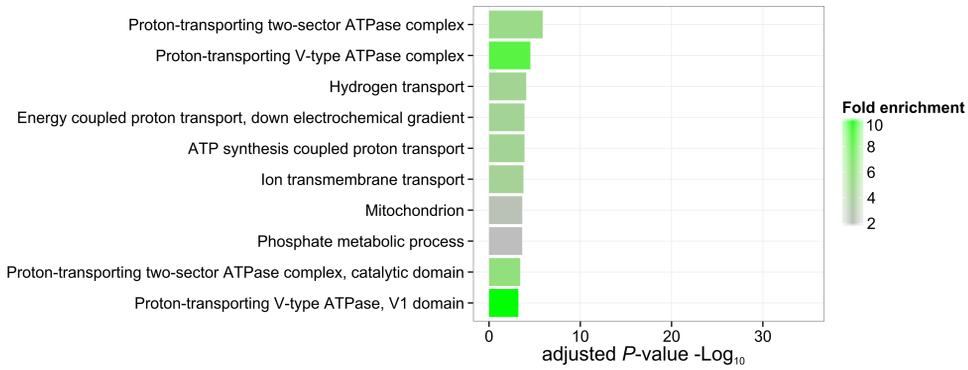
1038

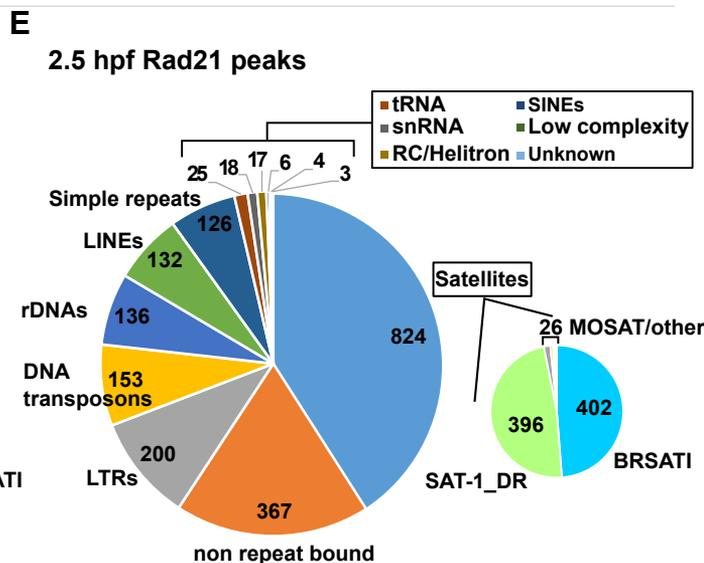
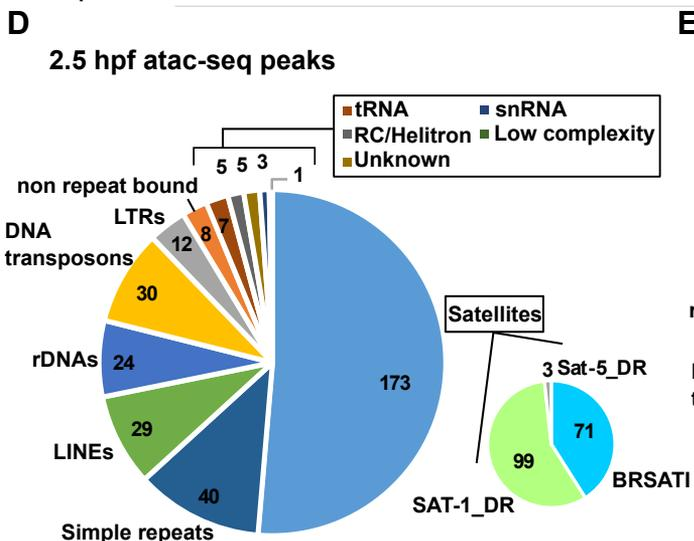
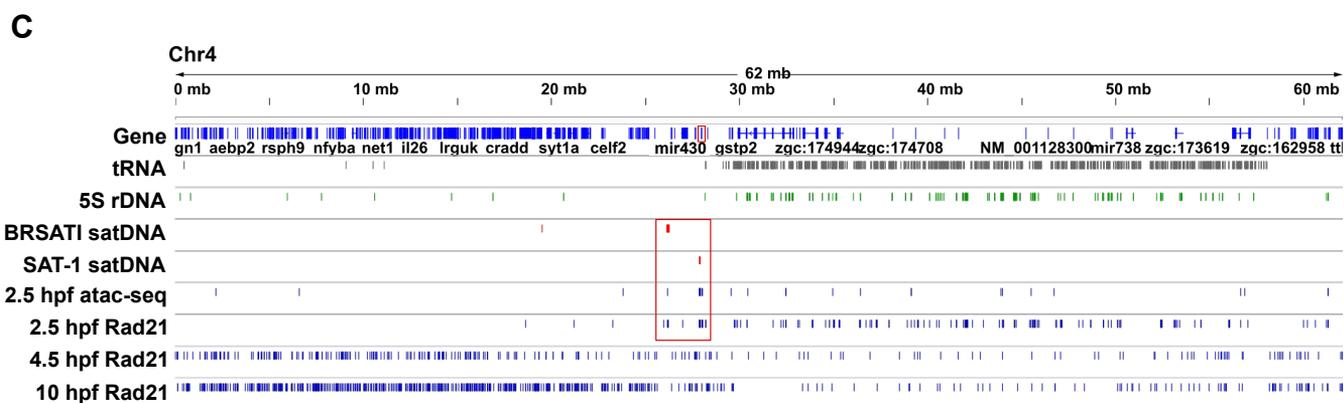
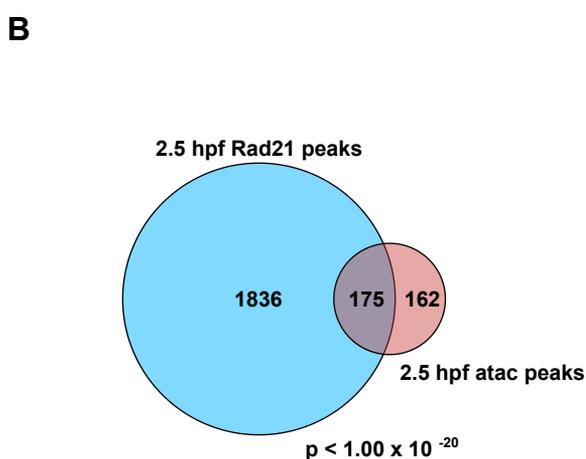
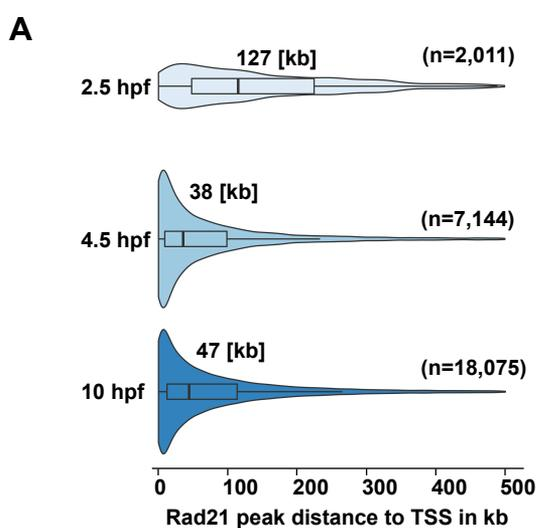


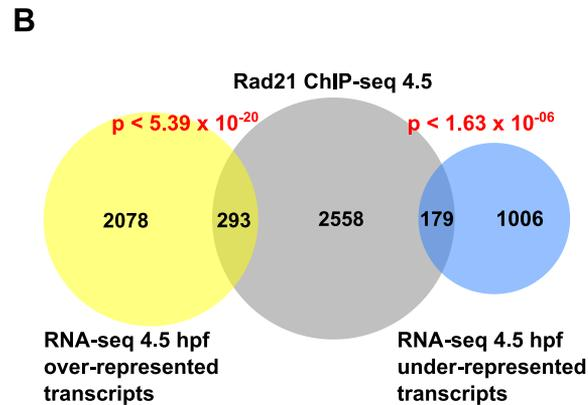
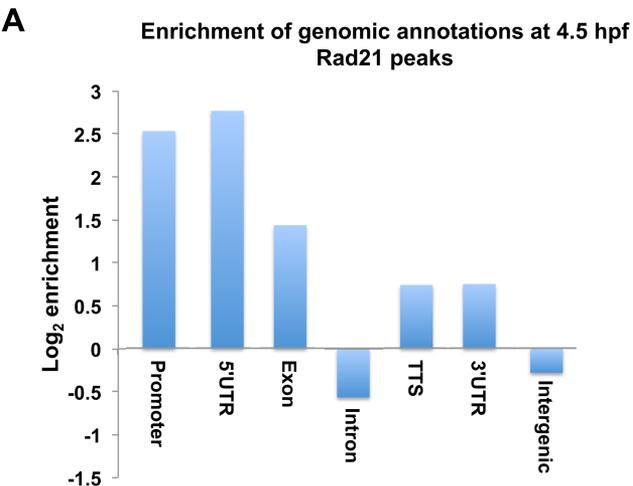


**A** Significantly reduced transcripts at 4.5 hpf**B** Significantly elevated transcripts at 4.5 hpf**C**

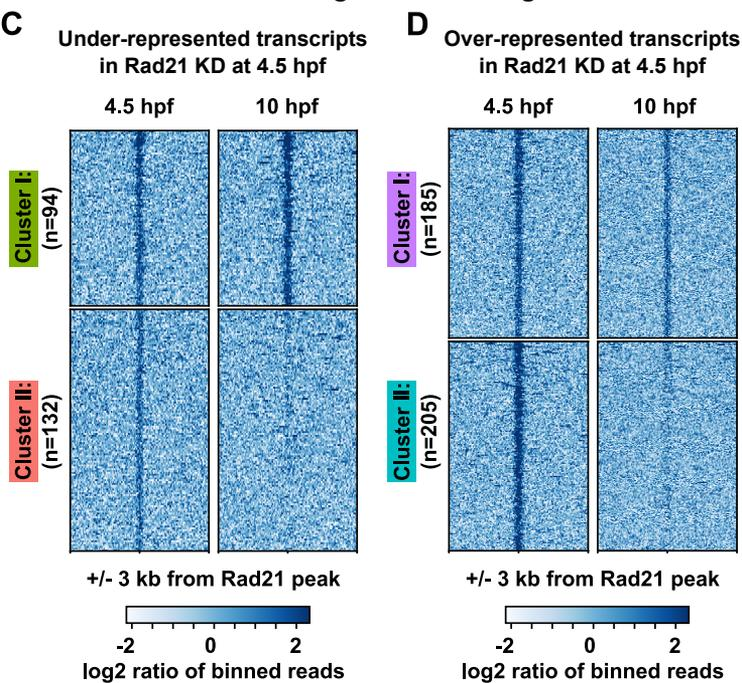


**A****B**

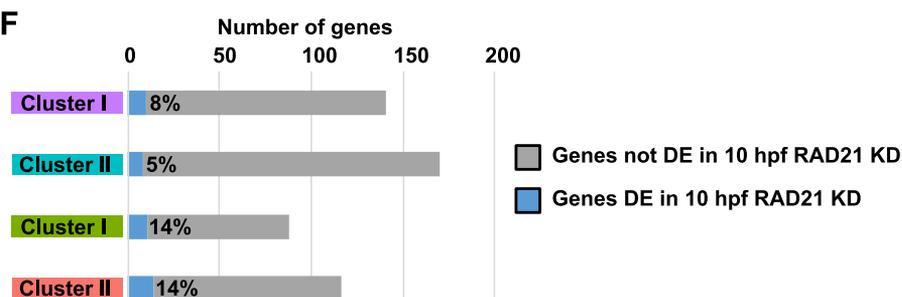
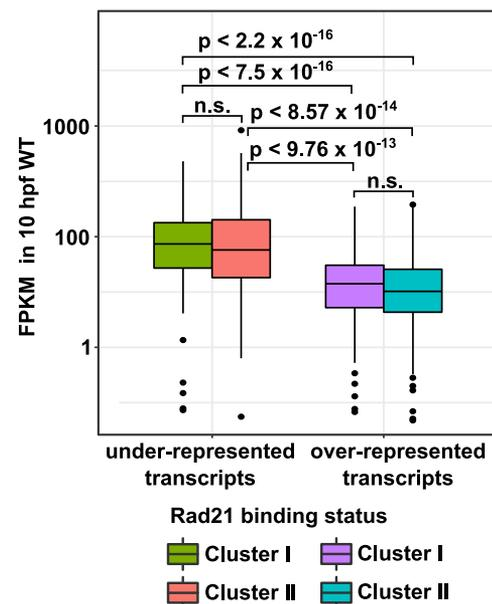


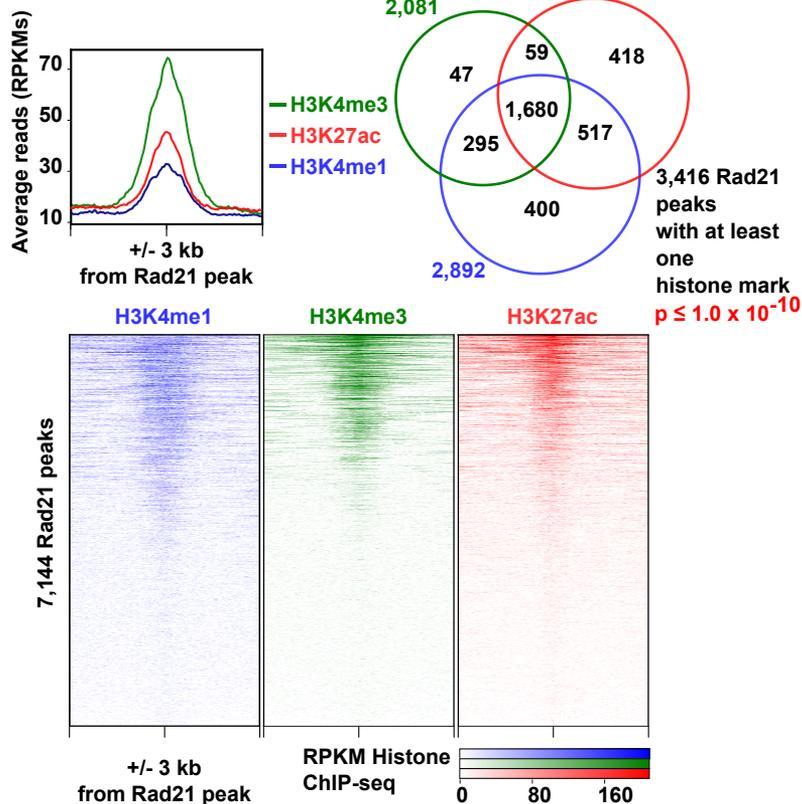
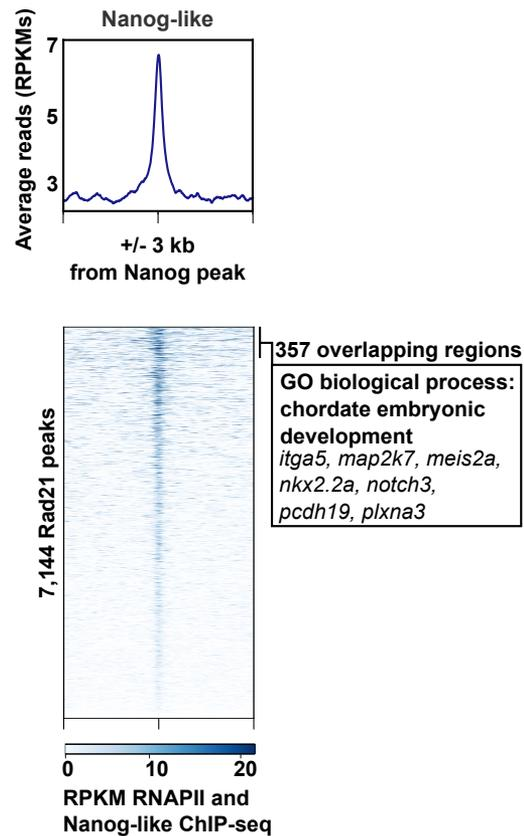
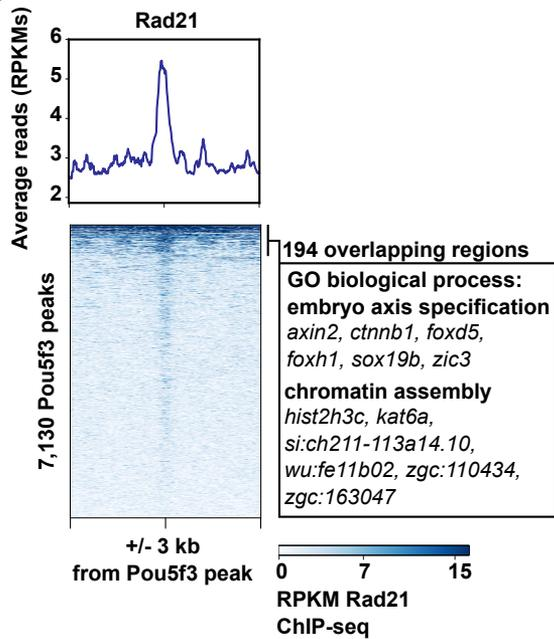
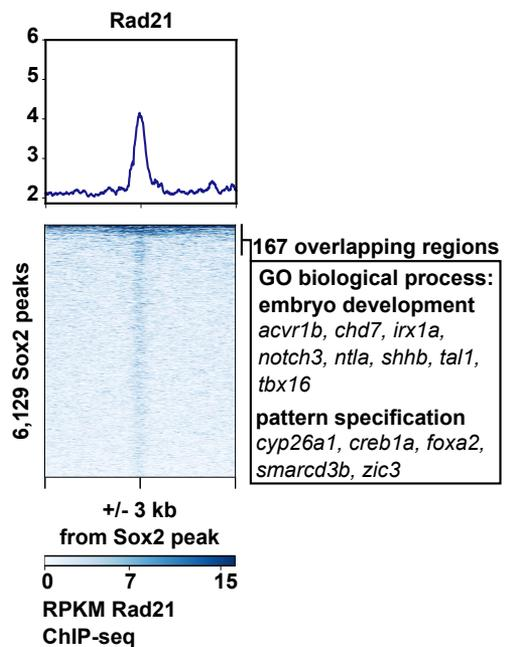


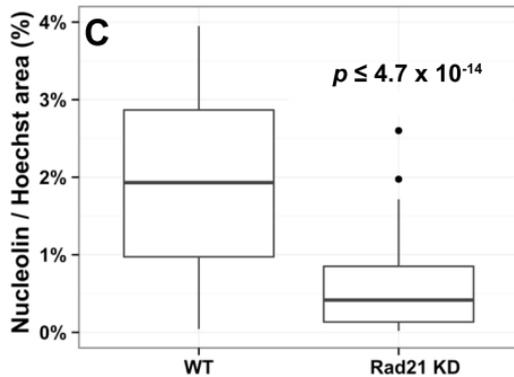
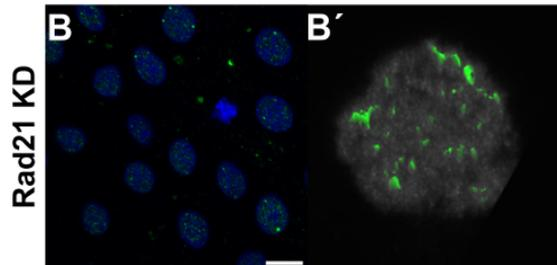
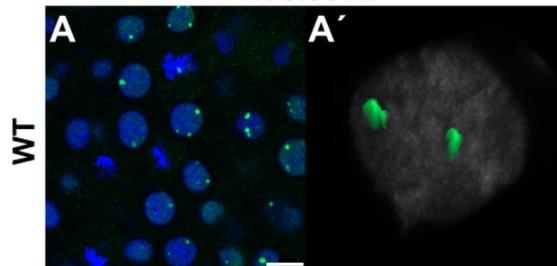
**Rad21 recruitment at genes encoding**



**E** Expression of 4.5 hpf Rad21 KD DE transcripts in 10 hpf WT embryos



**A****B****C****D**

**Nucleolin****pSer2-RNAPII**